Bacillus anthracis chain length, a virulence determinant, is regulated by a transmembrane Ser/Thr protein kinase PrkC

Neha Dhasmana[1¶], Nishant Kumar[1¶], Aakriti Gangwal[2¶], Chetkar Chandra Keshavam[2¶], Lalit K. Singh[1¶], Nitika Sangwan[2], Payal Nashier[2], Sagarika Biswas[1], Andrei P. Pomerantsev[3], Stephen H Leppla[3], Yogendra Singh[1,2#], and Meetu Gupta[1#]

[1]CSIR-Institute of Genomics and Integrative Biology, Mall Road, Delhi, India

[2]Department of Zoology, University of Delhi, Delhi, India

[3]Microbial Pathogenesis Section, Laboratory of Parasitic Diseases, National Institute of Allergy and Infectious Diseases, National Institutes of Health, Bethesda, Maryland, USA

[¶] These authors contributed equally

[#] For Correspondence – meetu.gupta@igib.in, yinghdu@gmail.com

Summary

Anthrax is a zoonotic disease caused by *Bacillus anthracis*, a spore-forming pathogen that displays a chaining phenotype. It has been reported that in a mouse infection model, systemic inoculation with longer bacterial chains caused blockade in lung capillaries. The blockade resulted in increased pathophysiological consequences viz, hypoxia and lung tissue injury. In this study, we identify the serine/threonine protein kinase of *B. anthracis*, PrkC, localized at the bacteria-host interface, as a determinant of bacterial chain length. *In vitro*, *prkC* disruption strain (BAS Δ*prkC*) grew as shorter chains throughout the bacterial growth cycle. BslO, a septal murein hydrolase, and Sap, an S-layer structural protein, required for the localization of BslO, were found to be upregulated in BAS Δ*prkC*. Additionally, we also observed a decrease in the cell wall thickness and an increase in multi-septa formation in BAS Δ*prkC*. During infection, PrkC may regulate the chaining phenotype through the identified signaling mechanism.

Introduction

Bacteria exhibit diverse shapes and morphologies, the result of long evolutionary processes that select genotypes best suited for bacterial survival. Apart from the variation in shape, bacteria display multi-cellular structures such as aggregates, biofilms, and chains/filaments (Yang et al., 2016; Young, 2006). *Bacillus anthracis*, the Gram-positive spore-forming pathogen of grazing mammals, and the etiological agent of anthrax grows as chains of rod-shaped cells (Koehler, 2009; Jouvion et al., 2016; Glomski et al., 2007b; Saile and Koehler, 2006). In the environment, *B. anthracis* persists primarily as metabolically inert oblong spores. Germination happens in the presence of an optimal signal within the host (Mock and Fouet, 2001). Emerging evidence indicates that spores can germinate, multiply and persist even outside their vertebrate host, in the presence of a nutrient-rich environment in the root

rhizosphere and simpler biological systems such as earthworm, housefly, and amoebae (Saile and Koehler, 2006, Schuch et al., 2010; Schuch and Fischetti, 2009; Dey et al., 2012; Fasanella et al., 2010].

B. anthracis spores can infect humans through three routes – gastrointestinal, inhalational, and cutaneous (Mock and Fouet, 2001; Beatty et al., 2003; Passalacqua et al., 2006; Doganay et al., 2010). The highest mortality rates are seen in inhalational anthrax (Spencer, 2003). Multiple factors act as virulence determinants (Moayeri et al., 2015; Sharma et al., 2017; Dhasmana et al., 2014). However, the secreted binary exotoxins (lethal toxin and edema toxin) and the anti-phagocytic poly-γ-D-glutamic acid capsule, encoded by the virulence plasmids pXO1 and pXO2, respectively, act as the primary virulence factors (Mock and Fouet, 2001; Mock and Mignot, 2003; Moayeri and Leppla, 2009). The exotoxins perturb host immune responses and cause toxemia, and the capsule prevents engulfment by phagocytes, resulting in septicemia (Moayeri and Leppla, 2009; Tournier et al., 2009).

Among other factors that play a role in virulence, the bacterial chaining phenotype has been shown to contribute significantly (Jouvion et al., 2016; Glomski et al., 2007b). During initial stages of infection, *B. anthracis* spores phagocytosed by macrophages, germinate, and grow in chains before causing cell rupture (Ruthel et al., 2004). In mice, the high pathogenicity of systemically inoculated *B. anthracis* strain making capsule but not the toxins (encapsulated but nontoxinogenic strain) was linked to chain length-dependent blockade of alveolar capillaries leading to hypoxia, lung tissue injury, and death (Jouvion et al., 2016; Glomski et al., 2007b). Of note, the lung is the terminal organ targeted by *B. anthracis*, irrespective of the route of infection (Glomski et al., 2007b; Glomski et al., 2007a; Dumetz et al., 2011). These studies indicate that the chaining phenotype presents a survival advantage to *B. anthracis* within its host during both early and late stages of infection.

Intrigued by the relevance of this morphotype in the biology of *Bacillus* species, various groups have tried to identify the mechanisms controlling bacterial chain length in both pathogenic and non-pathogenic strains (Huillet et at., 2017; Nguyen-Mau et al., 2012; Kern et al., 2012; Anderson et al., 2011; Kearns and Losick, 2005; Ababneh and Herman, 2015a; Ababneh and Herman, 2015b; Chai et al., 2010; Chen et al., 2009). In *B. anthracis*, one of the determinants of bacterial chain length is the septal peptidoglycan hydrolase, BslO (*bacillus* *s*urface *l*ayer *O*). BslO is a *Bacillus* *S*-*l*ayer associated protein (BSL) with *N*-acetylglucosaminidase activity that catalyzes daughter cell separation (Anderson et al., 2011). Restrictive deposition of BslO to the septal region is, in turn, attributed to sequential coverage of the cell wall by the primary S-layer proteins (SLPs), Sap (*s*urface *a*rray *p*rotein) and EA1 (*e*xtractable *a*ntigen *1*) (Kern et al., 2012). SLPs and BSLs associate with the pyruvylated secondary cell wall polysaccharides (SCWP) through their conserved S-layer homology domain (SLH) (Mesnage et al., 2000; Kern et al., 2010). While several enzymes that influence the chaining phenotype through their role in synthesis/modification of SCWPs and hence the attachment of SLPs to SCWPs have been identified in *B. anthracis* (Kern et al., 2010; Lunderberg et al., 2013), a sensory molecule with a potential to regulate the chaining phenotype, possibly through regulation of one of these factors, remains unknown.

Through this work, we identify *B. anthracis* PrkC, the only serine/threonine protein kinase (STPK) localized at the bacteria-host interface, as a determinant of bacterial chain length. We show that the *B. anthracis* Sterne 34F2 *prkC* mutant strain (BAS Δ*prkC*) is not able to attain a chaining phenotype throughout the bacterial growth cycle. Both BslO and Sap are found to be upregulated in BAS Δ*prkC*, which probably creates a condition that favors de-chaining. Additionally, PrkC is also shown to influence the bacterial cell division, possibly through the regulation of the cytoskeletal protein, FtsZ. Through this work, we propose that PrkC, a transmembrane kinase with a sensor domain, perceives growth permissive signals and

maintains the levels of the primary proteins involved in de-chaining to regulate the chaining phenotype.

Results

STPKs, earlier thought to be limited to eukaryotes, are now identified as integral components of the bacterial systems with a definite role in bacterial survival and pathogenesis (Pereira et al., 2011). In *B. anthracis*, three STPKs have been characterized, namely PrkC (BAS 3713), PrkD (BAS 2152), and PrkG (BAS 2037) (Arora et al., 2012; Shakir et al., 2010; Bryant-Hudson et al., 2011). Among these, PrkC is the only membrane-associated protein kinase (Shakir et al., 2010; Madec et al., 2002). The extracellular ligand-binding motif of PrkC is composed of peptidoglycan binding PASTA (*p*enicillin-binding proteins *a*nd *S*er/Thr kinase-*a*ssociated) repeats. Interaction of the PASTA domain with peptidoglycan was first demonstrated for PrkC, wherein it was shown to interact with peptidoglycan fragments generated by neighboring growing cells, thereby triggering germination of *B. subtilis* and *B. anthracis* spores (Shah et al., 2008). Apart from a role in germination, *B. subtilis* PrkC has been implicated in stationary phase processes, sporulation, germination, and biofilm formation (Madec et al., 2002; Gaidenko et al., 2002).

prkC disruption results in bacteria with shorter chain length

Previously, our group had shown that *B. anthracis* PrkC-mediated processes play an essential role in germination and biofilm formation (Arora et al., 2017; Virmani et al., 2019). Some of the components of the PrkC-mediated signaling cascade leading to these processes were identified (Arora et al., 2017; Virmani et al., 2019). Work done by other groups implicated *B. subtilis* PrkC in later stages of bacterial growth and germination (Madec et al., 2002; Shah et al., 2008; Gaidenko et al., 2002). Even though *prkC* is expressed maximally during the

logarithmic phase of *in vitro* growth, *prkC* deletion has never been reported to result in any apparent defect in morphology, viability, or growth during this phase in either *B. subtilis* or *B. anthracis* (Arora et al., 2012; Shakir et al., 2010; Bryant-Hudson et al., 2011; Madec et al., 2002; Gaidenko et al., 2002; Pompeo et al., 2016; Libby et al., 2015). PrkC is, however, recognized as an infection-specific kinase and is critical for *B. anthracis* survival in macrophages (Shakir et al., 2010; Bryant-Hudson et al., 2011).

While working on the *B. anthracis* Sterne 34F2 *prkC* mutant strain (BAS Δ*prkC*), we observed that logarithmic cultures of BAS Δ*prkC* allowed to stand at room temperature formed a compact pellet whereas the parental wild type strain (BAS WT) did not (Fig. 1A). The absence of PrkC was leading to the formation of a compact pellet. In a study on a *B. anthracis bslO* mutant strain, Anderson et al. had shown that compact pellets were formed when bacteria grew as shorter chains while loose pellets were formed when bacteria exhibited extensive chaining (Anderson et al., 2011). This suggested that the absence of PrkC might be leading to the shortening of bacterial chains. To validate this, exponentially growing BAS WT and BAS Δ*prkC* were visualized under a phase-contrast microscope. As shown in Fig. 1B, and Fig. 1-figure supplement 1A, disruption of *prkC* resulted in bacteria growing as shorter chains, and this phenotype was reversed in a *prkC*-complemented strain (BAS Δ*prkC*::*prkC*). Further, to determine if *prkC* disruption resulted in a defect in the cell morphology, viz; bulging, shrinking, or changes in cell width or shape, BAS WT, and BAS Δ*prkC* were examined by scanning electron microscope (SEM). However, as seen in Fig. 1C, and Fig. 1-figure supplement 1B, no morphological defect was apparent, apart from the shortening of bacterial chains, indicating that the *prkC* disruption influenced only chain length. In a study on PknB, a membrane-localized PASTA kinase from *Mycobacterium tuberculosis*, depletion, or over-expression of the kinase was shown to have a significant effect on bacterial morphology leading to cell death (Chawla et al., 2014).

Effect of *prkC* disruption on chaining morphotype during different phases of bacterial growth

If PrkC is the sensor molecule required for maintaining the chaining phenotype, its absence in the BAS Δ*prkC* strain would result in shorter chains throughout the bacterial growth cycle. To examine this and to provide a basis for our experiments, we first monitored the growth of the BAS WT strain through the entire growth cycle (Fig. 2A). To determine growth stage-specific changes in chaining phenotype, culture aliquots were taken out at indicated time points and observed under a phase-contrast microscope. As seen in Fig. 2C, Fig. 2-figure supplement 1 and Fig. 3, BAS WT exhibited extensive chaining until ~ OD ($A600_{nm}$) 3.0, at 4 hr, after which a sudden shortening of bacterial chains was observed. The average chain length at 4hr was measured as 115.90 (±46.271 S.D., n = 50) µm while at 5 hr it shortened to 63.53 (±20.1150 S.D., n = 50) µm (Fig. 3). Interestingly, this time point correlated with the end of the exponential phase and the start of the deceleration phase (Fig. 2A), a stage where bacterial replication rate starts decreasing owing to nutrient deprivation and accumulation of metabolic by-products (Pletnev et al., 2015). Next, to determine the effect of *prkC* disruption on chaining phenotype, similar growth curve analysis, and chain length determinations/measurements were carried out as described above (Fig. 2B, Fig. 2C, Fig. 2-figure supplement 1 and Fig. 3). As shown in Fig. 2C, Fig. 2-figure supplement 1 and Fig. 3, BAS Δ*prkC* grew as shorter chains throughout the growth cycle. Of note, we did observe some chaining in the BAS Δ*prkC* cultures during the lag phase (t = 2h, Fig. 2C and Fig. 2-figure supplement 1), which could be due to an insufficient number of the de-chaining molecule(s) synthesized at this stage or due to the time taken for the assembly of these molecules at the desired location. In the presence of PrkC, synthesis of these molecule(s) is probably downregulated to allow bacteria to grow as chains. These results indicate that PrkC senses growth permissive signal(s) and regulates the levels of

molecules associated with de-chaining to maintain the long-chain phenotype, a morphology found during nutrient abundance (Koehler, 2009; Anderson et al., 2011).

PrkC regulates the expression of Sap, EA1 and BslO

In *B. anthracis*, Sap, and then EA1 sequentially form monomeric paracrystalline bi-dimensional surface S-layers during exponential and stationary growth-phase, respectively (Kern et al., 2012; Mignot et al., 2002). The saturating presence of Sap and EA1 on the cell wall confines the S-layer associated protein BslO (with a similar SLH domain) to the septal region (Kern et al., 2012). Disruption of *sap* has been shown to cause chain length elongation mainly because in the absence of Sap, BslO is no longer restricted to the septal region and is hence incapable of carrying out murein hydrolysis effectively (Kern et al., 2012). To understand whether PrkC maintains chaining phenotype through modulating the levels of Sap, BslO, and EA1, their expression levels were determined at the indicated time points (Fig. 2A and 2B) in the BAS WT and BAS Δ*prkC* strains. As shown in Fig. 4A, *prkC* disruption resulted in the upregulation of Sap at most of the time points for which the samples were collected. In BAS WT, a sharp increase in expression was observed toward the end of the exponential growth phase {~ OD ($A600_{nm}$) 3, Time – 4 hr}, Fig. 4A, and Fig. 2A. Interestingly, the initial time points when the Sap expression was low were also the time points where long chains were observed (Time – 2 hr and 3 hr), Fig. 4A, Fig. 2C, Fig. 2-figure supplement 1 and Fig. 3. However, in BAS Δ*prkC* strain, Sap levels were found to be higher than the BAS WT strain even at the initial time points (Time – 2 hr and 3 hr), Fig. 4A. This probably formed the reason for the de-chaining observed in the BAS Δ*prkC* strain from the beginning of the growth cycle. These results are in agreement with the previous report, where the absence of Sap was shown to result in a long chain phenotype (Kern et al., 2012).

Next, we wanted to determine the levels of BslO in the BAS WT and BAS Δ*prkC* strains. Experiments were conducted in a similar manner, as described above. Interestingly, we observed a stable expression of BslO throughout the growth cycle in BAS WT (Fig. 4B). As per our understanding, this is the first report where the levels of BslO have been determined at various stages of bacterial growth. Previous studies have conclusively established the role of BslO in de-chaining and have identified it as the primary murein hydrolase driving the de-chaining process (Kern et al., 2012; Anderson et al., 2011). As observed for Sap, *prkC* disruption resulted in the upregulation of BslO at most of the time points for which the samples were collected (Fig. 4B). The results obtained for Sap and BslO indicated that an increase in the levels of Sap and BslO in the absence of PrkC might create a condition that is most suitable for de-chaining. Increased Sap would restrict BslO to the septal region, which would carry out de-chaining, and an increase in the levels of BslO would further add to this effect.

Further, we determined the levels of EA1, another structural S-layer protein, that shows its presence as the culture approaches the stationary phase (Kern et al., 2012; Mignot et al., 2002). As seen in Fig. 4C, EA1 levels in BAS Δ*prkC* were downregulated at most of the time points for which the samples were collected. Since Sap acts as a transcriptional repressor of *eag* (Kern et al., 2012; Mignot et al., 2002), this decrease can be due to the increased levels of Sap in the BAS Δ*prkC* strain (Fig. 3A).

Altogether, these results indicate that during bacterial growth, PrkC maintains an optimum level of BslO, Sap, and EA1 to maintain the chaining phenotype.

prkC disruption results in decreased cell wall width and cell septa thickness and increased multi-septa formation

Through the course of these experiments, we observed that BAS Δ*prkC* growth curve was not superimposable with BAS WT (Fig. 2A and 2B). This result was in contradiction with

the earlier reports wherein *B. anthracis prkC* disruption was shown have no effect on the bacterial growth *in vitro* (Shakir et al., 2010; Bryant-Hudson et al., 2011; Arora et al., 2017). To validate our observation, we carried out a comparative growth curve analysis with BAS WT and BAS Δ*prkC* until extended stationary phase. Interestingly, as shown in Fig. 5A, BAS Δ*prkC* strain showed an attenuated replication rate throughout the bacterial growth cycle. Disruption of chaining alone couldn't have caused the observed defect in growth. To identify the reason(s) for the observed defect, we carried out microscopic analysis at the ultrastructural level, and both BAS WT and BAS Δ*prkC* were subjected to transmission electron microscopy. Interestingly, at the ultrastructural level, an apparent decrease in the cell wall width and septal thickness was observed in the *prkC* disruption strain (mid-log phase) (Fig. 5B, Fig. 5-figure supplement 1, Fig. 5C). Additionally, we also observed an increase in multi-septa formation in the *prkC* disruption strain during later stages of bacterial growth through both confocal and transmission electron microscopy (Fig. 6A, Fig. 6B, Fig. 6C, Fig. 6-figure supplement 1). PASTA domain containing kinases from other bacterial species have been shown to play a role in the regulation of cell division machinery and cell wall homeostasis (Pensinger et al., 2018). We surmise that similar signaling mechanisms may be operational in *B. anthracis* as well.

FtsZ is a cytoskeletal protein of cell division machinery that localizes at mid-cell and forms the initial Z ring. It also serves as the scaffold for further assembly of cell-division machinery (Adams and Errington, 2009). STPKs from other bacterial systems have been shown to phosphorylate and regulate the activity of FtsZ (Thakur and Chakraborti, 2006; Schultz et al., 2009). Our initial results suggest that *ftsZ* is constantly upregulated in the *prkC* disruption strain (Fig. 6D). This probably formed the reason for an increase in multi-septa formation observed in the *prkC* disruption strain possibly due to the mislocalization of FtsZ. Further experiments are underway to delineate the PrkC-mediated signaling cascades, disruption of

which results in the observed defects in cell division, cell wall homeostasis, and multi-septa formation.

Discussion

Chaining phenotype acts as a virulence factor in several bacterial pathogens (Yang et al., 2016; Jouvion et al., 2016; Justice et al., 2008; Rodriguez et al., 2012; Prashar, 2013; Möller et al., 2012; Feinberg et al., 1999; Margulis et al., 1998). In *Legionella pneumophila*, chaining morphology helps the pathogen evade phagosomal killing by interfering with phagosomal morphogenesis (Prashar, 2013). In *Streptococcus pneumoniae*, bacteria growing as long chains display increased attachment and adherence to epithelial cell surfaces, possibly via multivalent binding sites (Rodriguez et al., 2012). *Bacillus cereus*, a close relative of *B. anthracis* and a cause of food-borne and opportunistic infections in humans, also displays a chaining phenotype and has been shown to attach to the invertebrate gut through long filaments (Feinberg et al., 1999; Margulis et al., 1998). In *B. anthracis*, in a mice model, chain-length-dependent physical sequestration of an encapsulated nontoxinogenic strain in lung capillaries is thought to result in hypoxia and associated lung tissue injury, leading to host death (Jouvion et al., 2016; Glomski et al., 2007b).

In this study on *B. anthracis* Sterne strain, we identify a transmembrane serine/threonine protein kinase, PrkC, with an extracellular sensory PASTA domain, as a determinant of chaining phenotype. Interestingly, PrkC homologs are found in all the above-mentioned chain-forming pathogens (Fig. S1). Though PASTA kinases do not necessarily carry out similar signaling processes across various bacterial species (Pereira et al., 2011; Manuse et al., 2016), it would be worthwhile to explore whether PASTA kinases of these pathogens also form the primary messenger molecule for maintaining chaining phenotype as

reported for *B. anthracis* in this study. Notably, PASTA motifs are unique to bacteria, and their absence in eukaryotes makes them an attractive drug target (Manuse et al., 2016).

B. anthracis PrkC is a key messenger molecule that plays a central role in various cellular processes including infection in macrophages, biofilm formation and germination (Shakir et al., 2010; Bryant-Hudson et al., 2011; Shah et al., 2008; Arora et al., 2017). We report for the first time that *prkC* disruption results in the attenuation of growth rate during *in vitro* culturing (Fig. 5A). Interestingly, none of the previous studies have reported an attenuation of growth on the disruption of *prkC* during *in vitro* growth, as observed in this study. We believe that this discrepancy could be due to the difference in the subtype of the Sterne strain used [*B. anthracis* Sterne strain 7702 (Shakir et al., 2010; Bryant-Hudson et al., 2011) vs. B. *anthracis* Sterne strain 34F2 {used in this study}] or differential growth conditions. Some of the growth curve kinetics have been performed in microplates (Bryant-Hudson et al., 2011), whereas we carried out this analysis under ambient growth conditions with enough headspace and aeration, as discussed in Materials and Methods. This makes us believe that under sub-optimal growth conditions and thus the absence of abundant growth permissive signal(s), the role of PrkC becomes redundant during *in vitro* growth. It will be worthwhile to determine the chaining phenotype of *B. anthracis* during different phases of bacterial growth under sub-optimal/limited aeration growth conditions.

In this study, we show that in the *prkC* disruption strain, S-layer protein, Sap, and septal *N*-acetylglucosaminidase, BslO, are upregulated. On the contrary, stationary phase S-layer protein, Ea1, shows downregulation (Fig. 4). S-layers are found in many bacterial species where they form a cell cover and play important roles such as - 1) act like exoskeleton/mechanical barrier, 2) function like a scaffold for surface molecules, 3) mediate adhesion, leading to auto-aggregation and coaggregation, 4) work as a molecular sieve and, 5) act as an immunomodulatory factor (Gerbino et al., 2015; Sara and Sleytr, 2000). In *B.*

anthracis, S-layer is made up of two primary structural proteins, Sap and EA1, and several S-layer-associated proteins called BSLs, that carry out diverse roles (Missiakas and Schneewind, 2017). Previous studies have shown that Sap levels rise until the onset of the stationary phase, and the EA1 amount is minimal during the logarithmic phase (Mignot et al., 2002). As Sap levels go down, EA1 is upregulated and replaces Sap as the primary constituent of S-layer in the stationary phase. Both Sap and EA1 act as the transcriptional repressors of the *eag* gene (Mignot et al., 2002). Our results also show a gradual decline in the Sap levels from late log phase onwards {~ OD ($A600_{nm}$) 5.0-6.0, Time – 6-8} (Fig. 4A and Fig. 2A). EA1 levels, as reported earlier, were minimal during lag phase and early exponential phase but increased gradually till the last point of measurement (Fig. 4C). Interestingly, BslO levels remained constant throughout the growth cycle in BAS WT, which implies that the stage/growth phase-dependent de-chaining in wild-type strain is primarily dependent on its localization, which in turn is controlled by the levels of Sap on the cell surface. Upregulation of both Sap and BslO in BAS Δ*prkC* strain would create a condition that would favor de-chaining from the initial stages of bacterial growth. Altogether, our results suggest that PrkC keeps a check on the levels of Sap, BslO, and Ea1 during optimum growth conditions, thereby maintaining the chaining phenotype.

In conclusion, through this study, we show that PrkC, the transmembrane kinase of *B. anthracis* with a sensor PASTA domain, regulates chaining phenotype. Since the disruption strain of PrkC shows decreased virulence in mice model of pulmonary anthrax (Shakir et al., 2010), it will be relevant to see if the observed effect is due to a difference in the chaining phenotype as shown in this report. If proven so, therapeutic intervention against PrkC could help in controlling bacterial chain size and hence the lung tissue injury and its pathophysiological consequences.

Materials and methods

Bacterial strains and growth conditions

Escherichia coli DH5α (Invitrogen) and SCS110 (Stratagene) strains were used for cloning and BL21-DE3 (Invitrogen) strain was used for expression of recombinant proteins. The final concentrations of the antibiotics used were: 100 μg/ml ampicillin, 25 μg/ml kanamycin and 150 μg/ml spectinomycin. LB broth (Difco) with appropriate antibiotic was used to grow bacterial cultures at 37˚C with proper aeration (1:5 head space) and constant shaking at 200 rpm. *B. anthracis* Sterne strain 34F2 (BAS WT) was obtained from Colorado Serum Company and *prkC* gene knockout strain (BAS Δ*prkC*) was a gift from Jonathan Dworkin, Department of Microbiology, Columbia University, USA. The details of the primers, plasmids and strains used in the study are provided in the supplementary tables (S1-S3).

Generation of *prkC* complement strain

The *prkC* gene and its promoter gene sequence were amplified using the primers – (P13-P16). These genes were subsequently cloned in the shuttle vector pYS5 (Singh et al., 1989) and the positive clone obtained was transformed in SCS110 cells prior to electroporation in the BAS Δ*prkC* strain using Bio-Rad Gene Pulser Xcell (2.5 kV, 400Ω, 25 μF using 0.2 cm Bio-Rad Gene Pulser cuvette). The complemented strain thus obtained after the screening was named BAS Δ*prkC::prkC*.

Cloning, gene expression, and protein purification

Genes for *sap*, *eag*, *bslO* and *groEL* were amplified using BAS genomic DNA as template and sequence specific primers (P5 and P6 - *sap*, P7 and P8 - *eag*, P9 and P10 - *groEL*, P11 and P12 - *bslO*). The amplified products thus obtained for *sap*, *eag* and *groEL* were cloned in pProExHtc vector (Invitrogen), while *bslO* gene was cloned in pET28a vector (Invitrogen).

The resulting plasmids encodes His_6 tagged fusion proteins. Plasmids were transformed into *E. coli* BL21 (DE3) and proteins were purified using affinity chromatography, as described described (Gupta et al., 2009). Briefly, overnight grown cultures were diluted in LB broth (1:50) with appropriate antibiotic - ampicillin (100 μg/ml) or kanamycin (25 μg/ml) and grown at 37°C, 200 rpm. Cultures were induced with 1 mM IPTG at OD ($A600_{nm}$) of 0.5 - 0.8 and incubated overnight at 16°C. After this cells were pelleted and re-suspended in sonication buffer [50 mM Tris-HCl (pH-8.5), 5 mM – β-mercaptoethanol, 1 mM Phenylmethylsulfonyl fluoride (PMSF), 1X protease inhibitor cocktail (Roche Applied Science, U.S.A.) and 300 mM NaCl] and sonicated (9 cycles- 20% amplitude, 10 sec on and 30 sec off). The recombinant proteins were purified by affinity purification using Ni-nitrilotriacetic acid (NTA) column and the final elution was done using 200 mM imidazole. Protein estimation was done using Pierce BCA Protein Assay kit (Thermo Fisher Scientific).

Generation of polyclonal antibodies against GroEL and BslO in mice, and Sap and EA1 in rabbit

For generation of polyclonal antibodies 30 μg of purified protein (GroEL and BslO) was used for injecting in three BALB/c mice and 500 μg of purified protein (Sap and EA1) was used for injecting in three rabbits for each protein. Antigens were emulsified in complete Freund's adjuvant (Sigma-Aldrich) in 1:1 ratio before subcutaneous injection in the animals. Production of antibody was stimulated at an interval of 21 days followed by two booster injections of 15 μg protein emulsified in incomplete Freund's adjuvant for mice and three booster injections of 250 μg protein emulsified in incomplete Freund's adjuvant for rabbits. Animals were bled to collect serum 14 days after the final injection and the antibody titer was calculated by ELISA and used accordingly for further experiments.

Growth Kinetics

BAS WT and BAS Δ*prkC* strains were grown overnight in LB broth at 37℃, 200 rpm. These overnight grown cultures were taken as inoculum for growth kinetics experiments. The secondary cultures were initiated at starting OD ($A600_{nm}$) of 0.001 in triplicates in LB broth at 37℃, 200 rpm (New Brunswick Innova 42 Incubator Shaker). Following this the OD ($A600_{nm}$) was monitored until around 64 hr at indicated intervals (Fig. 5A).

For lysate preparation and microscopy, the secondary cultures for both the strains were initiated similarly in triplicates from overnight grown cultures at starting OD ($A600_{nm}$) of 0.001. Culture samples were collected at different time points (2 hr, 3 hr, 4 hr, 5 hr, 6 hr, 7 hr, 8 hr, 9 hr, 10 hr, 14 hr, 18 hr, 22 hr, 26 hr, and 30 hr) for analysis and the corresponding OD ($A600_{nm}$) was plotted (Figure 2A and 2B).

Phase Contrast Microscopy

For phase-contrast microscopy 1 ml of culture samples from growing cells of BAS WT and BAS Δ*prkC* were collected at different time points as mentioned in above section. The cells were pelleted and washed thrice with phosphate buffer (pH 7.4) and resuspended in 100 µL buffer. The cells were then observed under a 100 x/1.4 oil DIC objective of Zeiss Axio Imager Z2 Upright Microscope. Images were captured using Axiocam 506 color camera equipped to the microscope and processed in ZEN 2 Pro software.

Quantitative Immunoblot Analysis

For immunoblot analysis, 5-10 ml bacillus culture was collected at different time points (2 hr, 3 hr, 4 hr, 5 hr, 6 hr, 7 hr, 8 hr, 9 hr, 10 hr, 14 hr, 18 hr, 22 hr, 26 hr, and 30 hr) from BAS WT and BAS Δ*prkC* cultures. The cell pellet obtained was washed with PBS buffer and re-suspended in 1 ml lysis buffer [200 mM Tris-HCl (pH 7.5), 1 mM EDTA, 150 mM NaCl, 1

mM PMSF, 5% glycerol, and 1X protease inhibitor cocktail (Roche Applied Science)]. After this, sonication of the bacterial pellets resuspended in the buffer was done (9 cycles- 20% amplitude, 10 sec on and 30 sec off). Protein estimation was done using Pierce BCA Protein Assay kit (Thermo Fisher Scientific). 5 μg protein lysate sample of each time point was prepared using SDS sample buffer containing 250 mM Tris-HCl (pH 6.8), 30% (v/v) glycerol, 10% SDS, 10 mM DTT and 0.05% (w/v) Bromophenol Blue. Samples were heated for 5 min at 95°C prior to loading on 12% polyacrylamide gels followed by transfer onto NC membrane (Millipore). 3% BSA in phosphate buffer saline (PBS) with 0.05% Tween 20 (PBST) was used for blocking the membranes overnight at 4°C. This was followed by washing with PBST (3 washes of 5 mins each). Membranes were then probed with antibodies specific to Sap protein (1:50,000) or BslO protein (1:10,000) or EA1 protein (1:50,000) for 1 hr followed by washes with PBST (5 washes of 5 min each). After this anti-rabbit IgG secondary antibody (for Sap and EA1) or anti-mouse IgG secondary antibody (for BslO) conjugated with horseradish peroxide (1:10,000 - Cell Signaling Technology) was used and the blots were incubated for another 60 min, followed by 3 PBST washings of 10 min each. Finally, SuperSignal West Pico PLUS Chemiluminescent substrate (Thermo Fisher Scientific) was used to detect the signal and it was visualised and quantified with the luminescent image analyser (Amersham Imager 600 or ImageLab6.0.1). The blots were then stripped using stripping buffer and probed similarly using anti-GroEL (1:50,000) and anti-mice IgG secondary antibody conjugated with horseradish peroxide (1:10,000 - Cell Signaling Technology) for normalising the loading pattern.

RNA extraction and Quantitative Real Time PCR

BAS WT and BAS Δ*prkC* strains were grown to mid-log and stationary phase in triplicates for RNA extraction following hot lysis method as described previously (Jahn et al.,

2008; Schmitt et al., 1990; Yang et al., 2011) with a few modifications. Cells were harvested at 6,000 x g for 15 min and the cell pellet was washed once with PBS and resuspended in 500 µL TRIzol® (Invitrogen) and frozen at -80°C until ready for further processing. The frozen samples were thawed in ice and RNA was extracted following the hot lysis method. Briefly the samples were mixed with 400 µL of buffer (50 mM Tris (pH 8.0), 1% SDS and 1mM EDTA) and 400 µL of zirconia beads treated with DEPC water. This suspension was incubated at 65 °C for 15 min with rigorous intermittent vortexing after every 5 min. Suspension was cooled in ice and mixed well with 100 µLof chloroform/ml of TRIzol. Separation of the aqueous phase containing RNA was done by centrifugation at 9500 × g for 15 min at 4 °C. RNA was precipitated from the aqueous phase by adding $LiCl_2$ (0.5M) and 3X ice-cold isopropanol followed by 2 hr incubation at -80°C. RNA pellet thus obtained by centrifugation at 16,000 × g for 20 min (4°C) was washed using 70% ethanol (Merck) and resuspended in nuclease-free water after air drying. RNA sample was then treated with DNase (Ambion) to remove any residual DNA contamination (according to the manufacturer's protocol). RNeasy mini kit (Qiagen) was used to obtain pure RNA using the manufacturer's protocol. cDNA was prepared using 1 µg of RNA using first-strand cDNA synthesis kit (Thermo Fisher) according to the protocol provided by the manufacturer. To analyse the expression of *ftsZ* gene, 2 µL of cDNA (diluted 10 times) was used for each time point (mid-log and stationary) along with gene-specific primer and SYBR Green master mix (Roche) in a 10 µL reaction according to the manufacturer's protocol. Reactions were run in triplicates along with no template control in a LightCycler® 480 Instrument II (Roche). The *rpoB* gene encoding for DNA-directed RNA polymerase subunit beta was used as housekeeping control (Qi et al., 2001). All the primers used were sequence-specific with a PCR product of 120 bp size.

Scanning Electron Microscopy

BAS WT and BAS Δ*prkC* strains were grown in LB broth at 37°C and harvested at mid-log phase and processed (Dubey et al., 2011). Briefly the bacterial culture was harvested at 12,000 x g at 4°C, and the pellet thus obtained was washed thrice using 0.1 M sodium phosphate buffer (pH-7.4). Karnovsky's fixative (2.5% glutaraldehyde (TAAB) + 2% paraformaldehyde (Sigma) in 0.1 M sodium phosphate buffer pH 7.4) was used to fix the bacterial samples overnight at 4°C. Fixed cells were again washed using sodium phosphate buffer and this step was repeated thrice to remove any residual fixative from the pellet. After this the pellets were again fixed using 1% osmium tetroxide for 20 min at 4°C. Sequential dehydration was then done for 30 min each using a range of ethanol (Merck) (30%, 50%, 70%, 80%(X 2), 90%, 100%(X 3) at 4°C. A critical point drying technique was used for drying the samples followed by gold coating of 10 nm using an aluminium stubs coated with agar sputter. Images were captured using Zeiss Scanning Electron Microscope EVO LS15 at 20 KV. Comprehensive imaging, processing and analysis were performed with Smart SEM software (Singh et al., 2015).

Transmission Electron Microscopy

BAS WT and BAS Δ*prkC* strains were grown in LB Broth at 37°C and harvested at mid-log and stationary phase and processed. Briefly the bacterial culture was harvested at 12,000 x g at 4°C, and the pellet thus obtained was washed thrice using 0.1 M sodium phosphate buffer (pH 7.4). Karnovsky's fixative containing 2.5% glutaraldehyde (TAAB) and 2% paraformaldehyde (Sigma) was made in 0.1 M sodium phosphate buffer pH 7.4 and was used for primary fixation of the cells overnight at 4°C. Fixed cells were again washed using sodium phosphate buffer and this step was repeated thrice to remove any residual fixative from the pellet. After this the pellets were again fixed using 1% osmium tetroxide for 20 min at 4°C. Sequential dehydration was then done for 30 min each using a range of acetone (Merck) (30%,

50%, 70%, 80% (X 2), 90%, 100% (X 3) at 4°C. For the clearing process and removal of dehydrating agent, absolute xylene (Merck) was used and the samples were subjected for bullet preparation using araldite resin mixture (TAAB). Following this infiltration was done by raising the concentration of the embedding medium and lowering the concentration of clearing agents gradually. The final bullets were prepared by curing at 55°C for 24 hr and for 48 hr at 65°C. Sectioning were obtained using Leica UC6 ultra-cut to make the grids which were then observed in FEI Tecnai G^2 Spirit at 200 KV (Singh et al., 2015).

Confocal microscopy to analyse multi septa formation

FM4-64 labelling was used to visualise multi-septa formation in BAS WT and BAS Δ*prkC* strains using fluorescence. LB agarose pads were prepared using AB gene frame (Fischer Scientific; 17*54 mm) on frosted glass slides (Corning Micro slide Frosted; 75*25 mm). To prepare agarose pad 3% low melting agarose (Sigma) were poured on these slides and left for solidification until further use. 1 µL of exponentially growing cultures of BAS WT and BAS Δ*prkC* strains diluted to an OD ($A600_{nm}$) = 0.035 were spread evenly on the agarose pads along with 1ug/ml FM4-64 dye for staining the cell membrane. Images were captured using Leica TCS SP8 confocal laser scanning microscope at 3 hr and 12 hr using 63x oil immersion objective (Sharma et al., 2016).

Phylogenetic Analysis

The amino acid sequences of PrkC protein in different pathogens: *Bacillus anthracis* Sterne, *Bacillus cereus, Legionella pneumophilia and Streptococcus pneumoniae* were procured from NCBI. These sequences were aligned using T-coffee tool (Madeira et al., 2019). These protein sequences were then used for generation of phylogenetic tree by Neighbor Joining analysis conducted by MEGA X (Saitou and Nei, 1987; Kumar et al., 2018; Stecher et

al., 2020). The representation of branch lengths is in units of evolutionary distances computed by Poisson correction method (Zuckerkandl and Pauling, 1965).

Statistical analysis

GraphPad Software (Prism 6) was used for all the statistical analyses. The statistical tests are indicated in the figure legends and the corresponding two-tailed *t*-test or ANOVA P-values are reported in the graphs wherever required. *, $p<0.05$; **, $p<0.01$; ***, $p<0.001$ and ****, $p<0.0001$ were considered significant results. Values indicated in the graphs represent mean ± SD, where n = 3 for both the strains at each time point, unless specified otherwise in the figure legend. Error bars are indicative of SD, n = 3. All the experiments were done in biological triplicates to ensure the reproducibility of the obtained data. Real time experiments (Fig. 6D) were done in biological and technical triplicates, while growth kinetics (Fig. 2A, Fig. 2B and Fig. 5A) and western blot analysis (Fig. 4) was done using biological triplicates. Separate flasks of the same strains are considered biological replicates, while technical replicates refer to multiple readings of the same sample.

Figure Legends

Figure-1: *prkC* disruption results in bacteria with short chain length. (A) Photograph of culture sediments in microcentrifuge tubes after standing incubation (9 hr) at room temperature of BAS WT (left) and BAS Δ*prkC* (right) grown in LB media. (B) Phase contrast images of BAS WT, BAS Δ*prkC* and BAS Δ*prkC*::*prkC* strains in mid-log phase. Cells were grown in LB broth at 37°C and 1 ml sample was taken from cultures in mid-log phase. Cells were pelleted and washed with PBS and visualised under 100x/1.4 oil DIC objective of Zeiss Axio Imager Z2 Upright Microscope. Scale bar represents 10 μm. (C) Scanning electron microscopy of BAS WT and BAS Δ*prkC* strains in mid-log phase. Cells were grown in LB broth at 37°C

and harvested in mid-log phase. These were then washed with 0.1 M sodium phosphate buffer and fixed with Karnovasky's fixative followed by 1% osmium tetroxide. A critical point drying technique was used for drying the samples followed by gold coating of 10 nm using an aluminium stubs coated with agar sputter. Cells were visualized under Zeiss Evo LS15. Scale bar represent 2 μm, magnification-5000X.

Figure 1 – figure supplement 1

(A) Representative phase contrast images of BAS WT, BAS Δ*prkC* and BAS Δ*prkC*::*prkC* strains in mid-log phase. Cells were visualized under 100x/1.4 oil DIC objective of Zeiss Axio Imager Z2 Upright Microscope. Scale bar represents 10 μm. (B) Representative scanning electron microscopy images of BAS WT and BAS Δ*prkC* strains to analyze morphological changes in cells growing in mid-log phase. Cells were visualized under Zeiss Evo LS15. Scale bar represent 2 μm (upper panel – Magnification 5000X) and 10 μm (lower panel – Magnification 3000X).

Figure-2: Effect of *prkC* disruption on chaining morphotype during different phases of bacterial growth. (A) Growth kinetics of BAS WT. BAS WT strain was grown in LB broth at 37°C. Absorbance [OD ($A600_{nm}$)] was recorded at the indicated time points. Error bars denote standard deviation, n = 3. (B) Growth kinetics of BAS Δ*prkC*. BAS Δ*prkC* strain was grown in LB broth at 37°C. Absorbance [OD ($A600_{nm}$)] was recorded at the indicated time points. Error bars denote standard deviation, n = 3. (C) Phase contrast images of BAS WT and BAS Δ*prkC* strains at different phases of bacterial growth cycle. Cells were grown at 37°C in LB broth and 1 ml sample was harvested at time points indicated in Fig. 2A and Fig. 2B. Cells were pelleted and washed with PBS and visualised under 100x/1.4 oil DIC objective of Zeiss Axio Imager Z2 Upright Microscope. Scale bar represents 10 μm.

Figure 2 – figure supplement 1

Phase contrast images of BAS WT and BAS Δ*prkC* strains at different phases of bacterial growth cycle. Cells were pelleted and washed with PBS and visualised under 100x/1.4 oil DIC objective of Zeiss Axio Imager Z2 Upright Microscope. Scale bar represents 10 μm.

Figure-3: Quantitative analysis of chain length variation in *prkC* disruption strain. Scatter dot plot denoting BAS WT and BAS Δ*prkC* strain chain length measurement during different phases of bacterial growth. Phase contrast images of BAS WT and BAS Δ*prkC* strains were used for measurement of the bacterial chain length using ImageJ software. Some data points in chain length quantitation (BAS WT – 2 hr, 3 hr and 4 hr) represent the maximum observable chain length obtained in the phase contrast images. Vertical and horizontal black line in the data set denotes SD and mean for both the strains at indicated time points, n = 50. These values are indicated in a separate table below the graph. Statistical significance of chain length distribution in BAS WT and BAS Δ*prkC* strains was analyzed using two-way ANOVA and denoted in the graph in the form of asterisk - *. P-values reported - *, $p<0.05$; **, $p<0.01$; ***, $p<0.001$ and ****, $p<0.0001$ were considered significant results.

Figure 3 – figure supplement 1

Detailed summary statistics table for Fig. 3.

Figure-4: PrkC regulates the expression of Sap, BslO and EA1. (A) Differential expression of Sap protein in BAS WT and BAS Δ*prkC* strains. Equal amount of protein at different time points (2 hr, 3 hr, 4 hr, 5 hr, 6 hr, 7 hr, 8 hr, 9 hr, 10 hr, 14 hr, 18 hr, 22 hr, 26 hr and 30 hr) was loaded onto SDS-PAGE, transferred onto nitrocellulose membrane and probed by Sap antibody (1:50,000) raised in rabbit. The same blot was then stripped and probed by GroEL

antibody (1:50,000) raised in mice. Densitometry analysis was done using ImageLab software and the ratio of Sap w.r.t. GroEL was used to plot a graph for showing differential expression of Sap protein in the BAS WT and BAS Δ*prkC* strain in a growth phase dependent manner. Error bars denote standard deviation, n = 3. Representative images are from one of the three independent experiments. (B) Differential expression of BslO protein in BAS WT and BAS Δ*prkC* strains. Equal amount of protein at different time points (2 hr, 3 hr, 4 hr, 5 hr, 6 hr, 7 hr, 8 hr, 9 hr, 10 hr, 14 hr, 18 hr, 22 hr, 26 hr and 30 hr) was loaded onto SDS-PAGE, transferred onto nitrocellulose membrane and probed by BslO antibody (1:10,000) raised in mice. The same blot was then stripped and probed by GroEL antibody (1:50,000) raised in mice. Densitometry analysis was done using the ImageLab software and the ratio of BslO w.r.t. GroEL was used to plot a graph for showing differential expression of BslO protein in the BAS WT and BAS Δ*prkC* strain in a growth dependent manner. Error bars denotes standard deviation, n = 3. Representative images are from one of the three independent experiments. (C) Differential expression of EA1 protein in BAS WT and BAS Δ*prkC* strains. Equal amount of protein at different time points (2 hr, 3 hr, 4 hr, 5 hr, 6 hr, 7 hr, 8 hr, 9 hr, 10 hr, 14 hr, 18 hr, 22 hr, 26 hr and 30 hr) was loaded onto SDS-PAGE, transferred onto nitrocellulose membrane and probed by EA1 antibody (1:50,000) raised in rabbit. The same blot was then stripped and probed by GroEL antibody (1:50,000) raised in mice. Densitometry analysis was done using ImageLab software and the ratio of EA1 w.r.t. GroEL was used to plot a graph for showing differential expression of EA1 protein in the BAS WT and BAS Δ*prkC* strain in a growth dependent manner. Error bars denotes standard deviation, n = 3. Representative images are from one of the three independent experiments.

Figure 4 – figure supplement 1

Immunoblot replicates for Sap, BslO and EA1 protein with their respective GroEL used as loading control for densitometer analysis. Equal amount of protein at different time points (2 hr, 3 hr, 4 hr, 5 hr, 6 hr, 7 hr, 8 hr, 9 hr, 10 hr, 14 hr, 18 hr, 22 hr, 26 hr and 30 hr) was loaded onto SDS-PAGE for BAS WT and BAS Δ*prkC* strains. These gels were then transferred onto nitrocellulose membrane and the same blots were probed by Sap, BslO, EA1 and GroEL antibody by stripping and re-probing protocol. "*" denotes same GroEL control blots for BAS WT Sap, BAS WT EA1 and BAS WT BslO, while "**" denotes same GroEL control blots for BAS Δ*prkC* Sap, BAS Δ*prkC* EA1 and BAS Δ*prkC* BslO.

Figure-5: *prkC* disruption results in decreased cell wall width and septa thickness. (A) Growth kinetics of BAS WT and BAS Δ*prkC* strains. Bacterial strains were grown in LB broth at 37°C till extended period of 65 hr. Absorbance [OD ($A600_{nm}$)] was recorded at the indicated time points. Error bars denote standard deviation, n = 3. Inset shows expanded growth profile of BAS WT and BAS Δ*prkC* strains up till 6 hr. (B) Transmission electron micrographs representing the ultrastructural details of difference in cell wall thickness and septum thickness of BAS WT and BAS Δ*prkC* strains. Cells were harvested at mid-log phase and primary fixation was done using Karnovasky's fixative. Secondary fixation was done using 1% osmium tetroxide and the samples were embedded into araldite resin mixture (TAAB). Scale bar represents 100 nm. (C) Bar graph representing the difference in cell wall thickness of BAS WT and BAS Δ*prkC* strains. Transverse sections of around 100 mid-log phase cells of each strain was used to calculate the cell wall thickness and plotted. Statistical significance of the data set was analysed using two-tailed Student's *t* test and denoted in the graph in the form of asterisk - *. P-values reported - *, $p<0.05$; **, $p<0.01$; ***, $p<0.001$ and ****, $p<0.0001$ were considered significant results.

Figure 5– figure supplement 1

Ultrastructural details of cell wall width and septa thickness of BAS WT and BAS Δ*prkC* in mid-log phase. Upper panel (A) represents longitudinal section, while lower panel (B) represents transverse sections of the bacilli. Scale bar represents 100 nm, Magnification – 11,500X.

Figure 5 – figure supplement 2

Detailed summary statistics table for Fig. 5C.

Figure-6: *prkC* disruption results in increased multi-septa formation. (A) Representative transmission electron microscopy images of BAS WT and BAS Δ*prkC* stationary phase cells showing multi- septa formation. Cells were harvested at stationary phase and primary fixation was done using Karnovasky's fixative. Secondary fixation was done using 1% osmium tetroxide and the samples were embedded into araldite resin mixture (TAAB). Scale bar represents 100 nm. (B) Staining of live bacterial cells with FM4-64 membrane stain. BAS WT and BAS Δ*prkC* strains grown up to exponential phase were diluted to an initial [OD ($A600_{nm}$)] = 0.035 and 1μL was spread on agarose pad. The pads were incubated at 37°C. Cell membrane was stained with FM4-64 (Final concentration of 1 μg/ml) and images were captured by Leica SP8 confocal microscope at 3 hr (above panel) and 12 hr (below panel). Arrows indicate the presence of multi-septa in the images. Scale bar represents 10μm. (C) Graph indicating ratio distribution of multi-septa formation with respect to the total number of cells in BAS WT and BAS Δ*prkC* strains at 3 hr and 12 hr. Around 1500 cells were considered for calculation of each bar in the graph.

(D) Comparative gene expression analysis of *ftsZ* gene in BAS Δ*prkC* strain as compared to BAS WT strain during mid-log and stationary phase. The data was normalized to the expression

of *rpoB* from each sample. Error bar represents an average of three biological and three technical replicates. Statistical significance of *ftsZ* gene expression in BAS WT and BAS Δ*prkC* strains at both the time points was analyzed using two-way ANOVA and denoted in the graph in the form of asterisk - *. P-values reported - *, $p<0.05$; **, $p<0.01$; ***, $p<0.001$ and ****, $p<0.0001$ were considered significant results.

Figure 6 – figure supplement 1

(A) Cell division anomalies during stationary cultures in BAS Δ*prkC* strains strain. Cells were harvested during stationary conditions and processed for TEM. Multi-septa were observed in the *prkC* mutant strain suggesting that accuracy of divisome machinery was lost and septum was formed at multiple locations. Scale bar represents 100nm, Magnification – 11,500X. (B) Staining of live bacterial cells with the FM4-64 membrane stain. BAS WT and BAS Δ*prkC* strains grown up to exponential phase were diluted to an initial [OD ($A600_{nm}$)] = 0.035 and 1μL was spread on agarose pad. The pads were incubated at 37°C. Cell membrane was stained with FM4-64 (Final concentration of 1μg/ml) and images were captured by Leica SP8 confocal microscope at 3 hr (above panel) and 12 hr (below panel). Arrows indicate the presence of multi-septa in the images. Scale bar represents 10μm.

Figure 6 – figure supplement 2

Detailed summary statistics table for Fig. 6D.

Supplementary Figure legends

Figure-S1. (A**)** Multiple sequence alignment of PrkC in different pathogenic bacteria (*Bacillus anthracis* Sterne, *Bacillus cereus, Legionella pneumophilia and Streptococcus pneumoniae)* using T-Coffee. The symbols used in the figure are indicative of: "*****" - perfect alignment, "**:**"

- strongly similar residues and **“.”** – weakly similar residues. (B) A phylogenetic tree representing the evolutionary relationship of PrkC in above mentioned pathogens. It was generated using Neighbor-Joining analysis conducted in MEGA X. The sequences used for alignment in panel A are included to generate the tree. The tree is drawn to scale with branch lengths.

Acknowledgements

This work was funded by SERB Grant No CRG/2018/000847/HS and J C Bose fellowship (SERB) to Yogendra Singh. Part of this work was done by ND at National Institutes of Health, Bethesda, MD, USA as a Fulbright Scholar. AG, CCK and NK are supported by University Grant Commission (UGC), NS is supported by Council of Scientific and Industrial Research (CSIR), PN is supported by SERB Grant and MG is supported by CSIR (SRA). We also thank Dr. Hemlata Gautam for technical guidance in scanning electron microscopy, CSIR-IGIB, Delhi and Sandip Arya, Anurag Singh, Raj Girish Mishra and other technical staff from Transmission Electron Microscope facility AIIMS, Delhi. We would also like to thank Dr A.K. Goel, Defense Research & Development Establishment, Gwalior for providing Sap and EA1 antibody and Hem Narayan Sharma, animal house staff, Department of Zoology, University of Delhi for help in GroEL and BslO antibody preparation. We are grateful to Dr. Anurag Agrawal, Director, CSIR-IGIB for support and providing the required facilities.

References

Ababneh, Q.O., and Herman, J.K. (2015a). CodY Regulates SigD Levels and Activity by Binding to Three Sites in the fla/che Operon. J. Bacteriol. *197*, 2999-3006. DOI:10.1128/JB.00288-15.

Ababneh, Q.O., and Herman, J.K. (2015b). RelA inhibits Bacillus subtilis motility and chaining. J. Bacteriol. *197*, 128-37. DOI:10.1128/JB.02063-14.

Adams, D.W., and Errington, J. (2009). Bacterial cell division: assembly, maintenance and disassembly of the Z ring. Nat. Rev. Microbiol. *7*, 642-53. DOI:10.1038/nrmicro2198.

Anderson, V.J., Kern, J.W., McCool, J.W., Schneewind, O., and Missiakas, D. (2011). The SLH-domain protein BslO is a determinant of Bacillus anthracis chain length. Mol. Microbiol. *81*, 192-205. DOI:10.1111/j.1365-2958.2011.07688.x.

Arora, G., Sajid, A., Arulanandh, M.D., Singhal, A., Mattoo, A.R., Pomerantsev, A.P., Leppla, S.H., Maiti, S., and Singh, Y. (2012). Unveiling the novel dual specificity protein kinases in Bacillus anthracis: identification of the first prokaryotic dual specificity tyrosine phosphorylation-regulated kinase (DYRK)-like kinase. J. Biol. Chem. *287*, 26749-63. DOI:10.1074/jbc.M112.351304.

Arora, G., Sajid, A., Virmani, R., Singhal, A., Kumar, C.M.S., Dhasmana, N., Khanna, T., Maji, A., Misra, R., Molle, V., Becher, D., Gerth, U., Mande, S.C., and Singh, Y. (2017). Ser/Thr protein kinase PrkC-mediated regulation of GroEL is critical for biofilm formation in Bacillus anthracis. NPJ Biofilms Microbiomes *3*, 7. DOI:10.1038/s41522-017-0015-4.

Beatty, M.E., Ashford, D.A., Griffin, P.M., Tauxe, R.V., and Sobel, J. (2003). Gastrointestinal anthrax: review of the literature. Arch. Intern. Med. *163*, 2527-31. DOI:10.1001/archinte.163.20.2527.

Bryant-Hudson, K.M., Shakir, S.M., and Ballard, J.D. (2011). Autoregulatory characteristics of a Bacillus anthracis serine/threonine kinase. J. Bacteriol. *193*, 1833-*42*. DOI:10.1128/JB.01401-10.

Chai, Y., Norman, T., Kolter, R., and Losick, R. (2010). An epigenetic switch governing daughter cell separation in Bacillus subtilis. Genes Dev. *24*, 754-65. DOI:10.1101/gad.1915010.

Chawla, Y., Upadhyay, S., Khan, S., Nagarajan, S.N., Forti, F., and Nandicoori, V.K. (2014). Protein kinase B (PknB) of Mycobacterium tuberculosis is essential for growth of the pathogen in vitro as well as for survival within the host. J. Biol. Chem. *289*, 13858-75. DOI:10.1074/jbc.M114.563536.

Chen, R., Guttenplan, S.B., Blair, K.M., and Kearns, D.B. (2009). Role of the sigmaD-dependent autolysins in Bacillus subtilis population heterogeneity. J. Bacteriol. *191*, 5775-84. DOI:10.1128/JB.00521-09.

Dey, R., Hoffman, P.S., and Glomski, I.J. (2012). Germination and amplification of anthrax spores by soil-dwelling amoebas. Appl. Environ. Microbiol. *78*, 8075-81. DOI:10.1128/AEM.02034-12.

Dhasmana, N., Singh, L. K., Bhaduri, A., Misra, R., & Singh, Y. (2014). Recent Developments in Anti-dotes Against Anthrax. Recent Pat. Antiinfect. Drug Discov., *9*, 83-96. DOI:10.2174/1574891x09666140830213925.

Doganay, M., Metan, G., and Alp, E. (2010). A review of cutaneous anthrax and its outcome. J. Infect. Public Health *3*, 98-105. DOI:10.1016/j.jiph.2010.07.004.

Dubey, G.P. and Ben-Yehuda, S. (2011). Intercellular nanotubes mediate bacterial communication. Cell *144*, 590-600. DOI:10.1016/j.cell.2011.01.015

Dumetz, F., Jouvion, G., Khun, H., Glomski, I.J., Corre, J.P., Rougeaux, C., Tang, W.J., Mock, M., Huerre, M., and Goossens, P.L. (2011). Noninvasive imaging technologies reveal edema toxin as a key virulence factor in anthrax. Am. J. Pathol. *178*, 2523-35. DOI:10.1016/j.ajpath.2011.02.027.

Fasanella, A., Scasciamacchia, S., Garofolo, G., Giangaspero, A., Tarsitano, E., and Adone, R. (2010). Evaluation of the house fly Musca domestica as a mechanical vector for an anthrax. PLoS One *5*, e12219. DOI:10.1371/journal.pone.0012219.

Feinberg, L., Jorgensen, J., Haselton, A., Pitt, A., Rudner, R., and Margulis, L. (1999). Arthromitus (Bacillus cereus) symbionts in the cockroach Blaberus giganteus: dietary influences on bacterial development and population density. Symbiosis *27*, 109-23. PubMed PMID: 11762374.

Gaidenko, T.A., Kim, T.J., and Price, C.W. (2002). The PrpC serine-threonine phosphatase and PrkC kinase have opposing physiological roles in stationary-phase Bacillus subtilis cells. J. Bacteriol. *184*, 6109-14. DOI:10.1128/jb.184.22.6109-6114.2002.

Gerbino, E., Carasi, P., Mobili, P., Serradell, M.A., and Gómez-Zavaglia, A. (2015). Role of S-layer proteins in bacteria. World J. Microbiol. Biotechnol. *31*, 1877-87. DOI:10.1007/s11274-015-1952-9.

Glomski, I.J., Corre, J.P., Mock, M., and Goossens, P.L. (2007a). Noncapsulated toxinogenic Bacillus anthracis presents a specific growth and dissemination pattern in naive and protective antigen-immune mice. Infect. Immun. *75*, 4754-61. DOI:10.1128/IAI.00575-07.

Glomski, I.J., Piris-Gimenez, A., Huerre, M., Mock, M., and Goossens, P.L. (2007b). Primary involvement of pharynx and peyer's patch in inhalational and intestinal anthrax. PLoS Pathog. *3*, e76. DOI:10.1371/journal.ppat.0030076.

Gupta, M., Sajid, A., Arora, G., Tandon, V., and Singh, Y. (2009). Forkhead-associated domain-containing protein Rv0019c and polyketide-associated protein PapA5, from substrates of serine/threonine protein kinase PknB to interacting proteins of Mycobacterium tuberculosis. J. Biol. Chem. *284*, 34723-34. DOI:10.1074/jbc.M109.058834.

Huillet, E., Bridoux, L., Wanapaisan, P., Rejasse, A., Peng, Q., Panbangred, W., and Lereclus, D. (2017). The CodY-dependent clhAB2 operon is involved in cell shape, chaining and autolysis in Bacillus cereus ATCC 14579. PLoS One *12*, e0184975. DOI:10.1371/journal.pone.0184975.

Jahn, C.E., Charkowski, A.O., and Willis, D.K. (2008). Evaluation of isolation methods and RNA integrity for bacterial RNA quantitation. J. Microbiol. Methods *75*, 318-24. DOI: 10.1016/j.mimet.2008.07.004.

Jouvion, G., Corre, J.P., Khun, H., Moya-Nilges, M., Roux, P., Latroche, C., Tournier, J.N., Huerre, M., Chrétien, F., and Goossens, P.L. (2016). Physical Sequestration of Bacillus anthracis in the Pulmonary Capillaries in Terminal Infection. J. Infect. Dis. *214*, 281-7. DOI:10.1093/infdis/jiw098.

Justice, S.S., Hunstad, D.A., Cegelski, L., and Hultgren, S.J. (2008). Morphological plasticity as a bacterial survival strategy. Nat. Rev. Microbiol. *6*, 162-8. DOI:10.1038/nrmicro1820.

Kearns, D.B., and Losick, R. (2005). Cell population heterogeneity during growth of Bacillus subtilis. Genes Dev. *19*, 3083-94. DOI:10.1101/gad.1373905.

Kern, J., Ryan, C., Faull, K., and Schneewind, O. (2010). Bacillus anthracis surface-layer proteins assemble by binding to the secondary cell wall polysaccharide in a manner that requires csaB and tagO. J. Mol. Biol. *401*, 757-75. DOI:10.1016/j.jmb.2010.06.059.

Kern, V.J., Kern, J.W., Theriot, J.A., Schneewind, O., and Missiakas, D. (2012). Surface-layer(S-layer) proteins sap and EA1 govern the binding of the S-layer-associated protein BslO at the cell septa of Bacillus anthracis. J. Bacteriol. *194*, 3833-40. DOI:10.1128/JB.00402-12.

Koehler, T.M. (2009). Bacillus anthracis physiology and genetics. Mol. Aspects Med. *30*:386-96. DOI:10.1016/j.mam.2009.07.004.

Kumar, S., Stecher, G., Li, M., Knyaz, C., and Tamura, K. (2018). MEGA X: Molecular Evolutionary Genetics Analysis across computing platforms. Mol. Biol. Evol. 35, 1547-1549. doi: 10.1093/molbev/msy096.

Libby, E.A., Goss, L.A., and Dworkin, J. (2015). The Eukaryotic-Like Ser/Thr Kinase PrkC Regulates the Essential WalRK Two-Component System in Bacillus subtilis. PLoS Genet. *11*, e1005275. DOI: 10.1371/journal.pgen.1005275.

Lunderberg, J.M., Nguyen-Mau, S.M., Richter, G.S., Wang, Y.T., Dworkin, J., Missiakas, D.M., and Schneewind, O. (2013). Bacillus anthracis acetyltransferases PatA1 and PatA2 modify the secondary cell wall polysaccharide and affect the assembly of S-layer proteins. J. Bacteriol. *195*, 977-89. DOI:10.1128/JB.01274-12.

Madec, E., Laszkiewicz, A., Iwanicki, A., Obuchowski, M., and Séror, S. (2002). Characterization of a membrane-linked Ser/Thr protein kinase in Bacillus subtilis, implicated in developmental processes. Mol. Microbiol. *46*, 571-86. DOI:10.1046/j.1365-2958.2002.03178.x.

Madeira, F., Park, Y.M., Lee, J., Buso, N., Gur, T., Madhusoodanan, N., Basutkar, P., Tivey, A.R.N., Potter, S.C., Finn, R.D., and Lopez, R. (2019). The EMBL-EBI search and sequence analysis tools APIs in 2019. Nucleic Acids Res. 47, 636-641. doi:10.1093/nar/gkz268.

Manuse, S., Fleurie, A., Zucchini, L., Lesterlin, C., and Grangeasse, C. (2016). Role of eukaryotic-like serine/threonine kinases in bacterial cell division and morphogenesis. FEMS Microbiol. Rev. *40*, 41-56. DOI: 10.1093/femsre/fuv041.

Margulis, L., Jorgensen, J.Z., Dolan, S., Kolchinsky, R., Rainey, F.A., and Lo, S.C. (1998). The Arthromitus stage of Bacillus cereus: intestinal symbionts of animals. Proc. Natl. Acad. Sci. U S A. *95*, 1236-41. DOI:10.1073/pnas.95.3.1236.

Mesnage, S., Fontaine, T., Mignot, T., Delepierre, M., Mock, M, and Fouet, A. (2000). Bacterial SLH domain proteins are non-covalently anchored to the cell

surface via a conserved mechanism involving wall polysaccharide pyruvylation. EMBO J. *19*, 4473-84. DOI:10.1093/emboj/19.17.4473.

Mignot, T., Mesnage, S., Couture-Tosi, E., Mock, M., and Fouet, A. (2002). Developmental switch of S-layer protein synthesis in Bacillus anthracis. Mol. Microbiol. *43*, 1615-27. DOI:10.1046/j.1365-2958.2002.02852.x.

Missiakas, D., and Schneewind, O. (2017). Assembly and Function of the Bacillus anthracis S-Layer. Annu. Rev. Microbiol. *71*, 79-98. DOI: 10.1146/annurev-micro-090816-093512.

Moayeri, M., and Leppla, S.H. (2009). Cellular and systemic effects of anthrax lethal toxin and edema toxin. Mol. Aspects Med. *30*, 439-55. DOI:10.1016/j.mam.2009.07.003.

Moayeri, M., Leppla, S.H., Vrentas, C., Pomerantsev, A.P., and Liu, S. (2015). Anthrax Pathogenesis. Annu. Rev. Microbiol. *69*, 185-208. DOI:10.1146/annurev-micro-091014-104523.

Mock, M., and Fouet, A. (2001). Anthrax. Annu. Rev. Microbiol. *55*, 647-71. DOI:10.1146/annurev.micro.55.1.647.

Mock, M., and Mignot, T. (2003). Anthrax toxins and the host: a story of intimacy. Cell Microbiol. *5*, 15-23. DOI:10.1046/j.1462-5822.2003.00253.x.

Möller, J., Luehmann, T., Hall, H., and Vogel, V. (2012). The race to the pole: how high-aspect ratio shape and heterogeneous environments limit phagocytosis of filamentous Escherichia coli bacteria by macrophages. Nano Lett. *12*, 2901-5. DOI: 10.1021/nl3004896.

Nguyen-Mau, S.M., Oh, S.Y., Kern, V.J., Missiakas, D.M., and Schneewind, O. (2012). Secretion genes as determinants of Bacillus anthracis chain length. J. Bacteriol. *194*, 3841-50. DOI:10.1128/JB.00384-12.

Passalacqua, K.D., and Bergman, N.H. (2006). Bacillus anthracis: interactions with the host and establishment of inhalational anthrax. Future Microbiol. *1*, 397-415. DOI:10.2217/17460913.1.4.397.

Pensinger, D.A., Schaenzer, A.J., and Sauer, J.D. (2018). Do Shoot the Messenger: PASTA Kinases as Virulence Determinants and Antibiotic Targets. Trends Microbiol. *26*, 56-69. DOI: 10.1016/j.tim.2017.06.010.

Pereira, S.F., Goss, L., and Dworkin, J. (2011). Eukaryote-like serine/threonine kinases and phosphatases in bacteria. Microbiol. Mol. Biol. Rev. *75*, 192-212. DOI:10.1128/MMBR.00042-10.

Pletnev, P., Osterman, I., Sergiev, P., Bogdanov, A., and Dontsova, O. (2015). Survival guide:Escherichia coli in the stationary phase. Acta Naturae *7*, 22-33. PubMed PMID: 26798489.

Pompeo, F., Foulquier, E., and Galinier, A. (2016). Impact of Serine/Threonine Protein Kinases on the Regulation of Sporulation in Bacillus subtilis. Front. Microbiol. *7*, 568. DOI: 10.3389/fmicb.2016.00568.

Prashar, A., Bhatia, S., Gigliozzi, D., Martin, T., Duncan, C., Guyard, C., and Terebiznik, M.R. (2013). Filamentous morphology of bacteria delays the timing

of phagosome morphogenesis in macrophages. J. Cell Biol. *203*, 1081-97. DOI:10.1083/jcb.201304095.

Qi, Y., Patra, G., Liang, X., Williams, L.E., Rose, S., Redkar, R.J., and DelVecchio, V.G. (2001). Utilization of the rpoB gene as a specific chromosomal marker for real-time PCR detection of Bacillus anthracis. Appl. Environ. Microbiol. *67*, 3720-7. DOI:10.1128/AEM.67.8.3720-3727.2001.

Rodriguez, J.L., Dalia, A.B., and Weiser, J.N. (2012). Increased chain length promotes pneumococcal adherence and colonization. Infect. Immun. *80*, 3454-9. DOI: 10.1128/IAI.00587-12.

Ruthel, G., Ribot, W.J., Bavari, S., Hoover, T.A. (2004). Time-lapse confocal imaging of development of Bacillus anthracis in macrophages. J. Infect. Dis. *189*, 1313-6. DOI:10.1086/382656.

Saile, E., and Koehler, T.M. (2006). Bacillus anthracis multiplication, persistence, and genetic exchange in the rhizosphere of grass plants. Appl. Environ. Microbiol. *72*, 3168-74. DOI:10.1128/AEM.72.5.3168-3174.2006.

Saitou, N., and Nei, M. (1987). The neighbor-joining method: A new method for reconstructing phylogenetic trees. Mol Biol Evol. 4, 406-425. doi:10.1093/oxfordjournals.molbev.a040454

Sára, M., and Sleytr, U.B. (2000). S-Layer proteins. J. Bacteriol. *182*, 859-68. DOI:10.1128/jb.182.4.859-868.2000.

Schmitt, M.E., Brown, T.A., and Trumpower, B.L. (1990). A rapid and simple method for preparation of RNA from Saccharomyces cerevisiae. Nucleic Acids Res. *18*, 3091-2. DOI:10.1093/nar/18.10.3091.

Schuch, R., and Fischetti, V.A. (2009). The secret life of the anthrax agent Bacillus anthracis: bacteriophage-mediated ecological adaptations. PLoS One *4*, e6532. DOI: 10.1371/journal.pone.0006532.

Schuch, R., Pelzek, A.J., Kan, S., and Fischetti, V.A. (2010). Prevalence of Bacillus anthracis-like organisms and bacteriophages in the intestinal tract of the earthworm Eisenia fetida. Appl. Environ. Microbiol. *76*, 2286-94. DOI:10.1128/AEM.02518-09.

Schultz, C., Niebisch, A., Schwaiger, A., Viets, U., Metzger, S., Bramkamp, M., and Bott, M. (2009). Genetic and biochemical analysis of the serine/threonine protein kinases PknA,PknB, PknG and PknL of Corynebacterium glutamicum: evidence for non-essentiality and for phosphorylation of OdhI and FtsZ by multiple kinases. Mol. Microbiol. *74*, 724-41. DOI: 10.1111/j.1365-2958.2009.06897.x.

Shah, I.M., Laaberki, M.H., Popham, D.L., and Dworkin, J. (2008) A eukaryotic-like Ser/Thr kinase signals bacteria to exit dormancy in response to peptidoglycan fragments. Cell *135*, 486-96. DOI:10.1016/j.cell.2008.08.039.

Shakir, S.M., Bryant, K.M., Larabee, J.L., Hamm, E.E., Lovchik, J., Lyons, C.R., and Ballard, J.D. (2010). Regulatory interactions of a virulence-associated serine/threonine phosphatase-kinase pair in Bacillus anthracis. J. Bacteriol. *192*, 400-9. DOI: 10.1128/JB.01221-09.

Sharma, A.K., Arora, D., Singh, L.K., Gangwal, A., Sajid, A., Molle, V., Singh, Y., and Nandicoori, V.K. (2016). Serine/Threonine Protein Phosphatase PstP of Mycobacterium tuberculosis Is Necessary for Accurate Cell Division and Survival of Pathogen. J. Biol. Chem. 291, 24215-24230. DOI:10.1074/jbc.M116.754531.

Sharma, A.K., Dhasmana, N., Dubey, N., Kumar, N., Gangwal, A., Gupta, M., and Singh, Y. (2017). Bacterial Virulence Factors: Secreted for Survival. Indian J. Microbiol. *57*, 1-10. DOI: 10.1007/s12088-016-0625-1.

Singh, L.K., Dhasmana, N., Sajid, A., Kumar, P., Bhaduri, A., Bharadwaj, M., Gandotra, S., Kalia, V.C., Das, T.K., Goel, A.K., Pomerantsev, A.P., Misra, R., Gerth, U., Leppla, S.H., and Singh, Y. (2015). clpC operon regulates cell architecture and sporulation in Bacillus anthracis. Environ. Microbiol. *17*, 855-65. DOI: 10.1111/1462-2920.12548.

Singh, Y., Chaudhary, V.K., and Leppla, S.H. (1989). A deleted variant of Bacillus anthracis protective antigen is non-toxic and blocks anthrax toxin action in vivo. J. Biol. Chem. *264*, 19103-7. PubMed PMID: 2509473.

Spencer, R.C. (2003). Bacillus anthracis. J. Clin. Pathol. *56*, 182-7. DOI:10.1136/jcp.56.3.182.

Stecher, G., Tamura, K., and Kumar, S. (2020). Molecular Evolutionary Genetics Analysis (MEGA) for macOS. Mol Biol. Evol. doi: 10.1093/molbev/msz312.

Thakur, M., and Chakraborti, P.K. (2006). GTPase activity of mycobacterial FtsZ is impaired due to its transphosphorylation by the eukaryotic-type Ser/Thr kinase, PknA. J. Biol. Chem. *281*, 40107-13. DOI:10.1074/jbc.M607216200.

Tournier, J.N., Rossi, Paccani. S., Quesnel-Hellmann, A., and Baldari, C.T. (2009). Anthrax toxins: a weapon to systematically dismantle the host immune defenses. Mol. Aspects Med. *30*, 456-66. DOI:10.1016/j.mam.2009.06.002.

Virmani, R., Sajid, A., Singhal, A., Gaur, M., Joshi, J., Bothra, A., Garg, R., Misra, R., Singh, V.P., Molle, V., Goel, A.K., Singh, A., Kalia, V.C., Lee, J.K., Hasija, Y., Arora, G., and Singh, Y. (2019). The Ser/Thr protein kinase PrkC imprints phenotypic memory in Bacillus anthracis spores by phosphorylating the glycolytic enzyme enolase. J. Biol. Chem. *294*, 8930-8941. DOI: 10.1074/jbc.RA118.005424.

Yang, D.C., Blair, K.M., and Salama, N.R. (2016). Staying in Shape: the Impact of Cell Shape on Bacterial Survival in Diverse Environments. Microbiol. Mol. Biol. Rev. *80*, 187-203. DOI:10.1128/MMBR.00031-15.

Yang, F., Tan, H., Zhou, Y., Lin, X., and Zhang, S. (2011). High-quality RNA preparation from Rhodosporidium toruloides and cDNA library construction therewith. Mol. Biotechnol. *47*, 144-51. DOI: 10.1007/s12033-010-9322-1.

Young, K.D. (2006). The selective value of bacterial shape. Microbiol. Mol. Biol Rev. *70*, 660-703. DOI:10.1128/MMBR.00001-06.

Zuckerkandl, E., and Pauling, L. (1965). Evolutionary divergence and convergence in proteins. Edited in Evolving Genes and Proteins by V. Bryson and H.J. Vogel, pp. 97-166. Academic Press, New York. doi: org/10.1016/B978-1-4832-2734-4.50017-6.

Figure 1

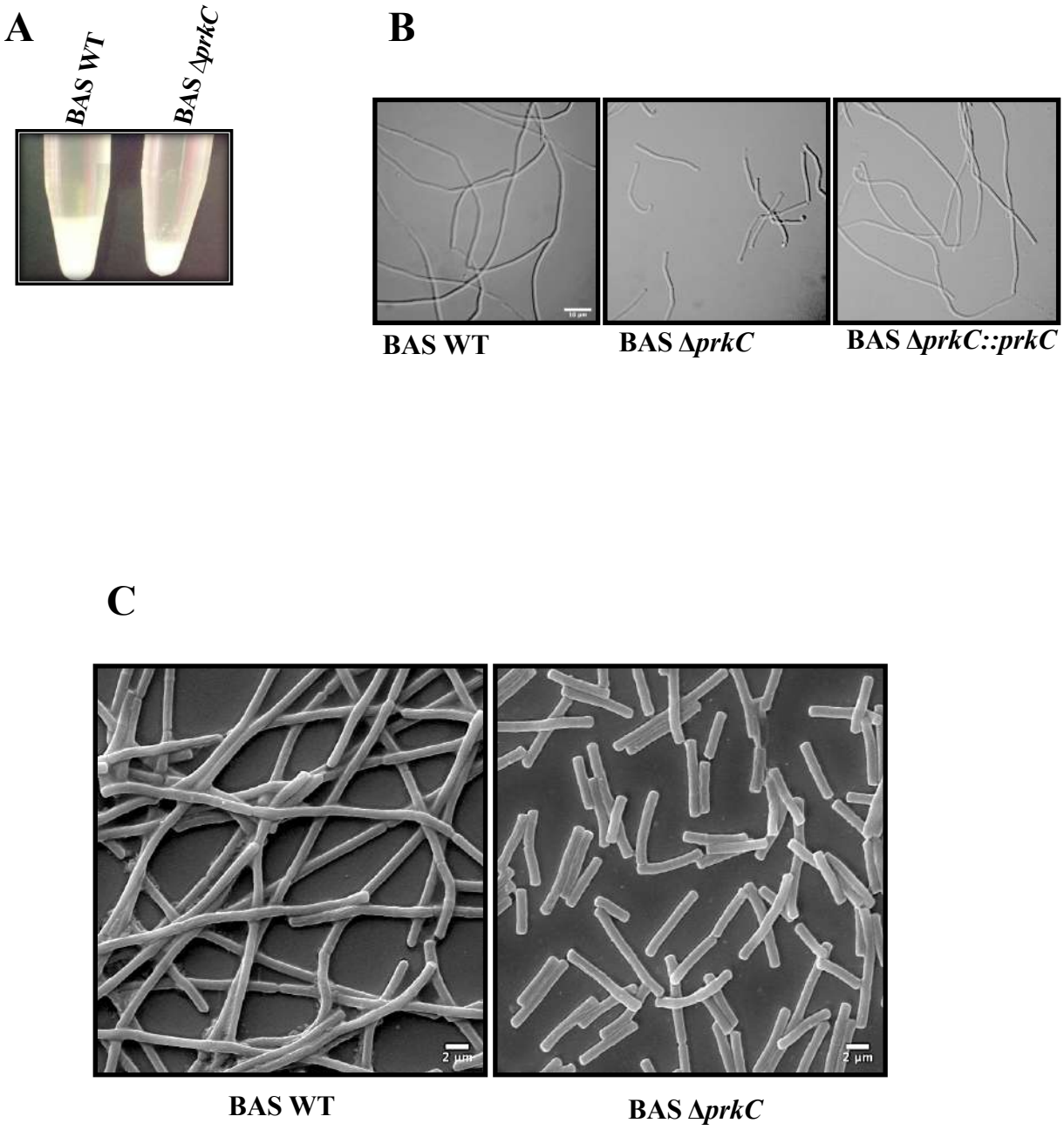
A
BAS WT
BAS ΔprkC
B
BAS WT
BAS ΔprkC
BAS ΔprkC::prkC
C
2 µm
2 µm
BAS WT
BAS ΔprkC

Figure 1 – figure supplement 1

A

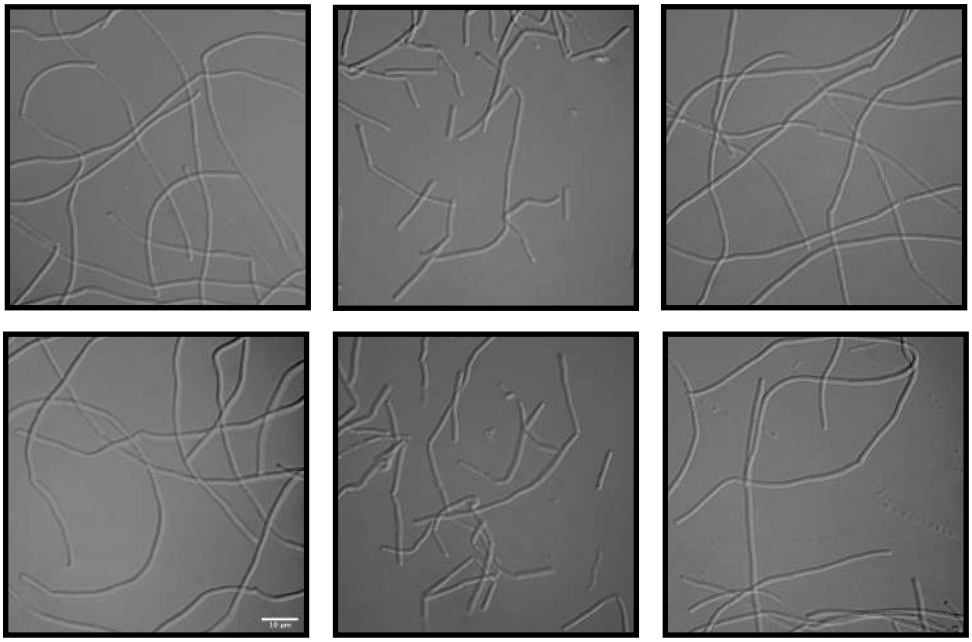

BAS WT **BAS Δ*prkC*** **BAS Δ*prkC::prkC***

B

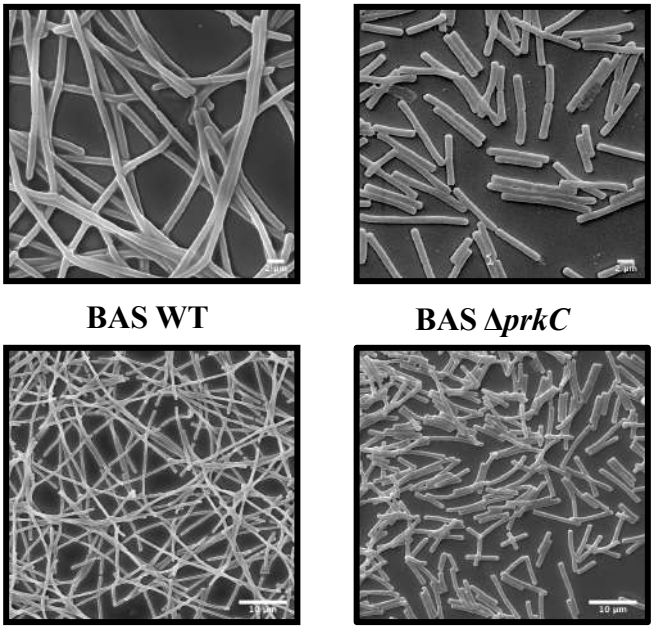

BAS WT **BAS Δ*prkC***

Figure 2

A

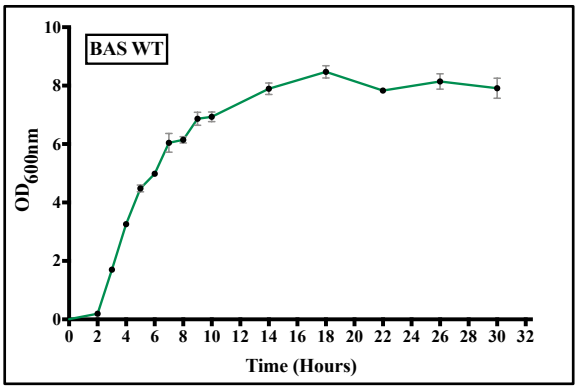
BAS WT
OD600nm
Time (Hours)
0
2
4
6
8
10
0 2 4 6 8 10 12 14 16 18 20 22 24 26 28 30 32

B

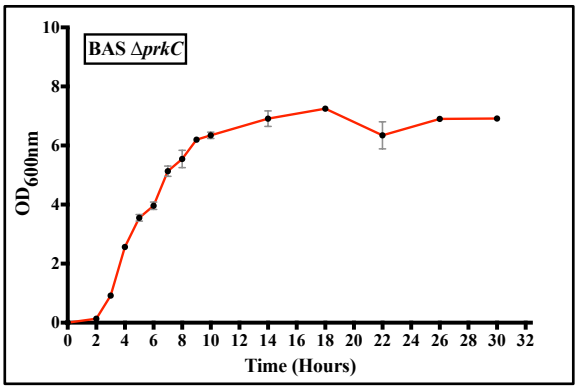
BAS ΔprkC
OD600nm
Time (Hours)
0
2
4
6
8
10
0 2 4 6 8 10 12 14 16 18 20 22 24 26 28 30 32

C

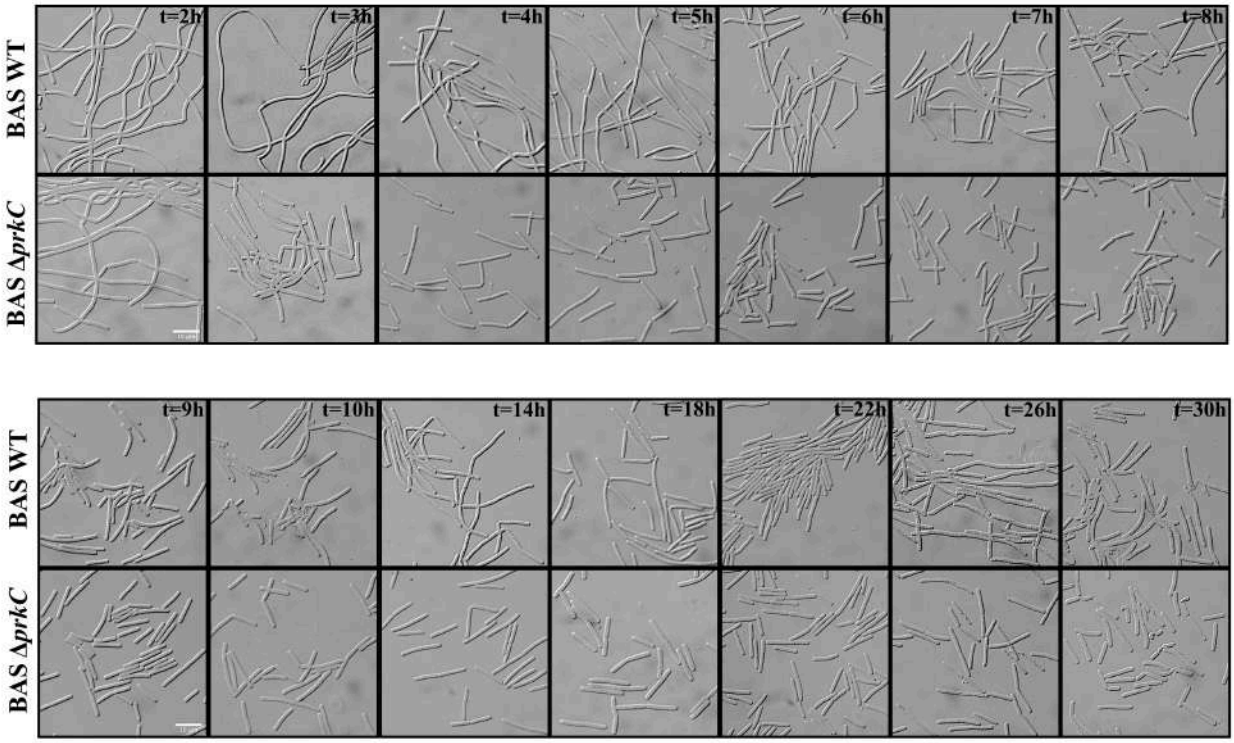
BAS WT
BAS ΔprkC
t=2h
t=3h
t=4h
t=5h
t=6h
t=7h
t=8h
t=9h
t=10h
t=14h
t=18h
t=22h
t=26h
t=30h

Figure 2 – figure supplement 1

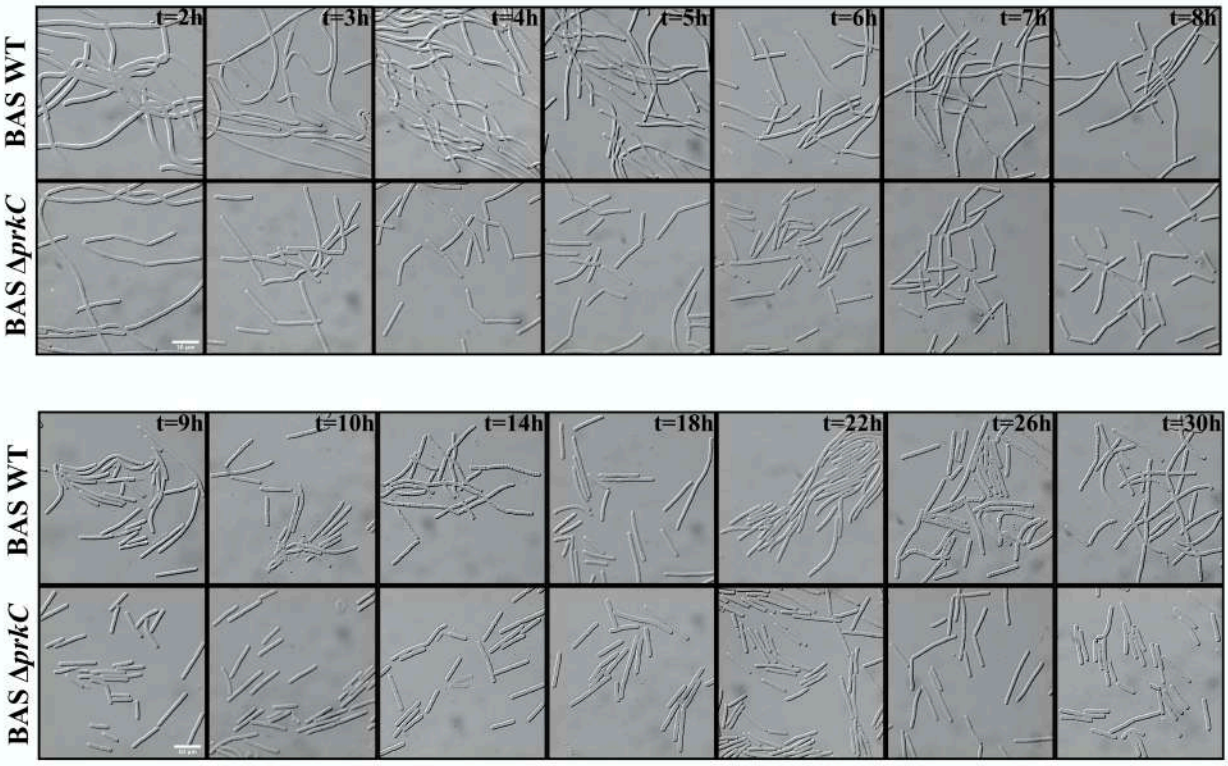

Figure 3

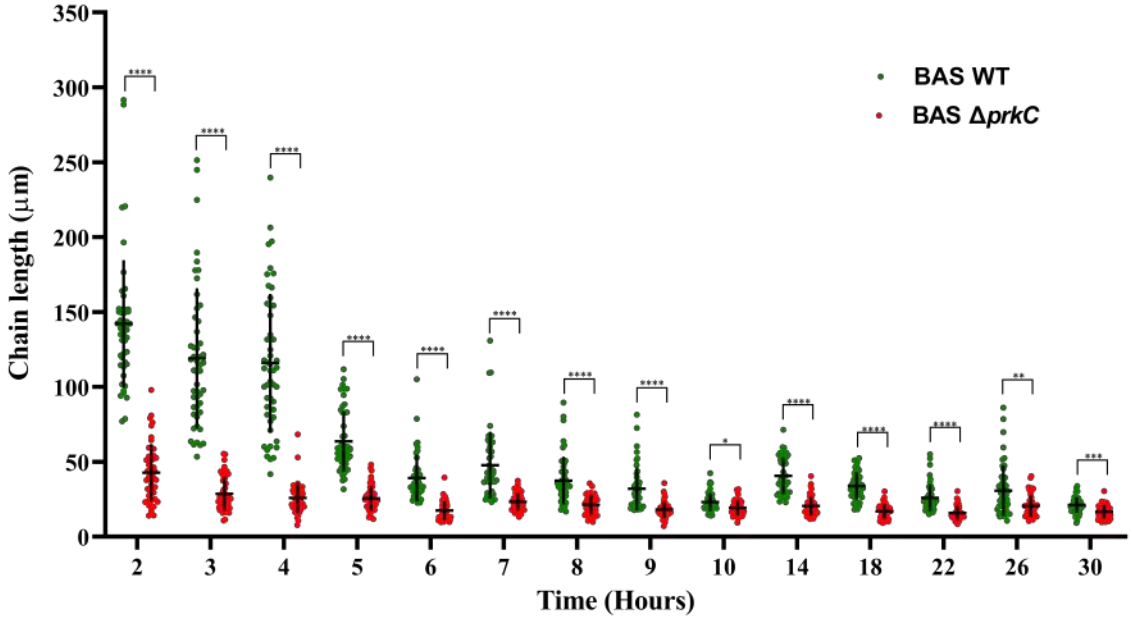

Time (Hours)	BAS WT		BAS Δ*prkC*	
	Mean (µm)	SD	Mean (µm)	SD
2	142.1084	42.6069	42.6963	19.1364
3	119.02844	46.8723	28.64966	11.3389
4	115.90408	46.2711	25.8465	9.9983
5	63.53988	20.1150	25.55476	8.3986
6	39.13004	15.5104	17.339	6.2770
7	47.77336	22.3645	23.18334	5.6947
8	37.32332	16.0714	21.22696	6.4880
9	31.93754	14.3880	18.00352	5.2235
10	23.02086	5.8793	19.27986	4.8745
14	40.57046	12.1721	20.49596	6.3195
18	33.85694	8.9581	16.8685	5.0875
22	25.77132	8.8618	15.8682	4.6959
26	30.69216	16.8488	20.43188	7.2795
30	21.10478	5.2186	16.62496	4.4415

Figure 3 – figure supplement 1

Figure 3 : Summary statistics			
BAS WT-BAS Δ*prkC* (Hours)	**95% CI of Difference**	**Summary**	**Adjusted P Values**
2	79.53 to 119.3	****	<0.0001
3	69.67 to 111.1	****	<0.0001
4	69.71 to 110.4	****	<0.0001
5	28.69 to 47.28	****	<0.0001
6	14.65 to 28.93	****	<0.0001
7	14.68 to 34.50	****	<0.0001
8	8.703 to 23.49	****	<0.0001
9	7.393 to 20.47	****	<0.0001
10	0.5219 to 6.960	*	0.0112
14	14.25 to 25.90	****	<0.0001
18	12.62 to 21.36	****	<0.0001
22	5.646 to 14.16	****	<0.0001
26	2.440 to 18.08	**	0.0026
30	1.592 to 7.368	***	0.0002

Figure 4

A

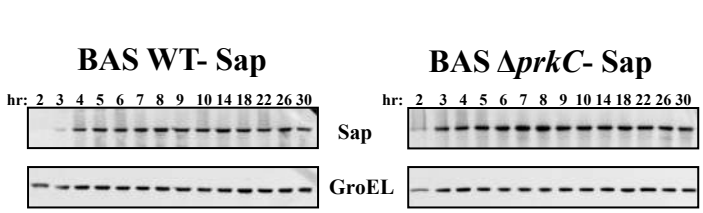
BAS WT- Sap
BAS Δ*prkC*- Sap
hr: 2 3 4 5 6 7 8 9 10 14 18 22 26 30
Sap
GroEL

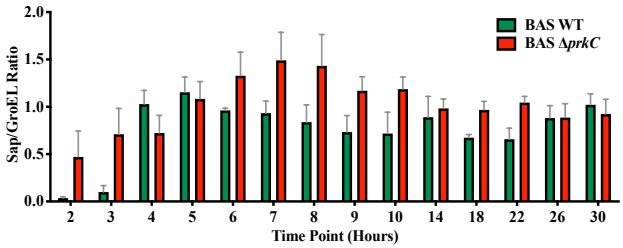
BAS WT
BAS Δ*prkC*
Sap/GroEL Ratio
0.0
0.5
1.0
1.5
2.0
2 3 4 5 6 7 8 9 10 14 18 22 26 30
Time Point (Hours)

B

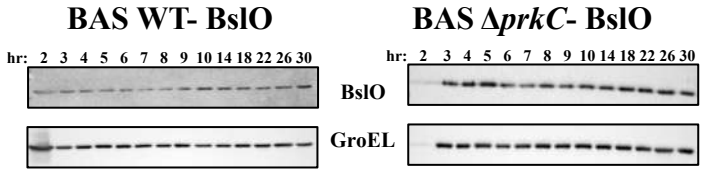
BAS WT- BslO
BAS Δ*prkC*- BslO
hr: 2 3 4 5 6 7 8 9 10 14 18 22 26 30
BslO
GroEL

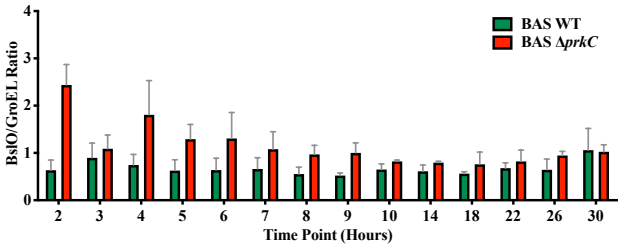
BAS WT
BAS Δ*prkC*
BslO/GroEL Ratio
0
1
2
3
4
2 3 4 5 6 7 8 9 10 14 18 22 26 30
Time Point (Hours)

C

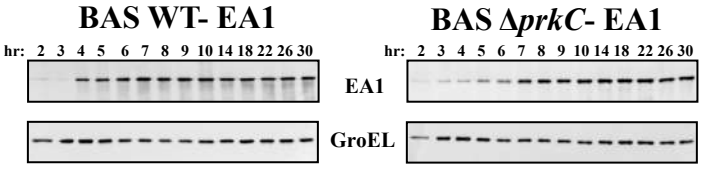
BAS WT- EA1
BAS Δ*prkC*- EA1
hr: 2 3 4 5 6 7 8 9 10 14 18 22 26 30
EA1
GroEL

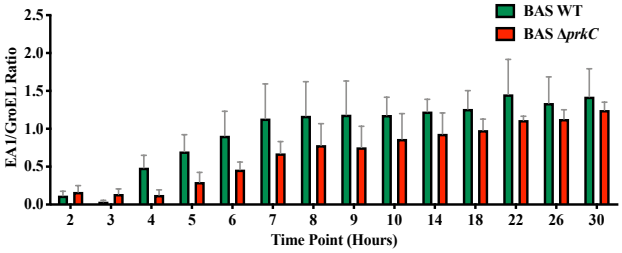
BAS WT
BAS Δ*prkC*
EA1/GroEL Ratio
0.0
0.5
1.0
1.5
2.0
2.5
2 3 4 5 6 7 8 9 10 14 18 22 26 30
Time Point (Hours)

Figure 4 – figure supplement 1

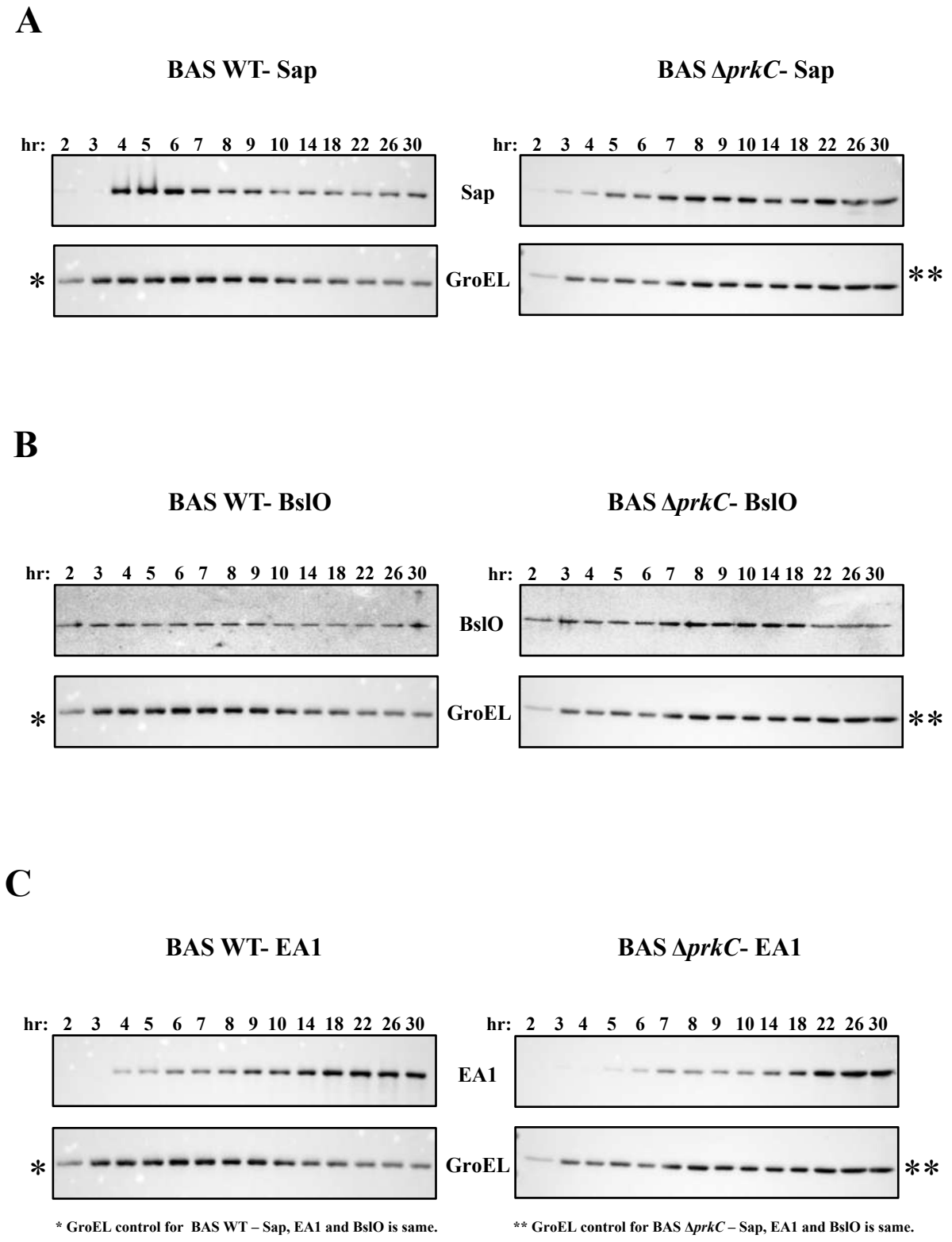

* GroEL control for BAS WT – Sap, EA1 and BslO is same.

** GroEL control for BAS Δ*prkC* – Sap, EA1 and BslO is same.

Figure 5

A

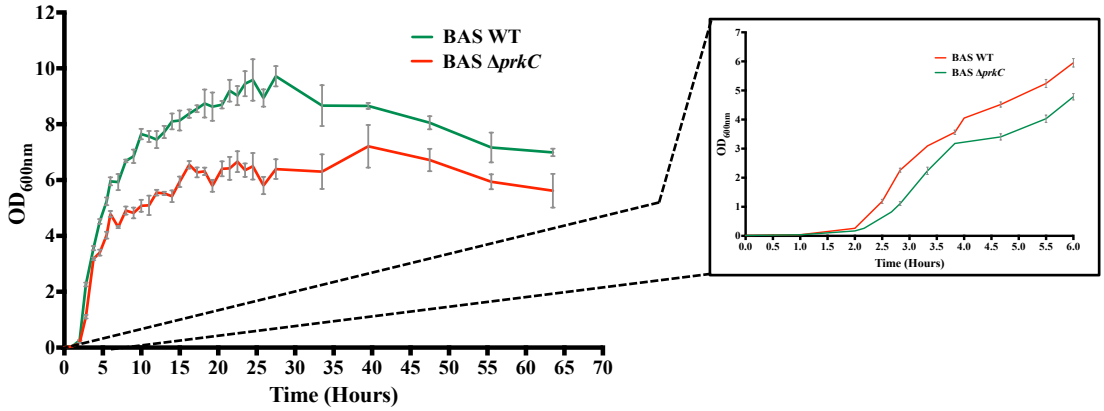

B

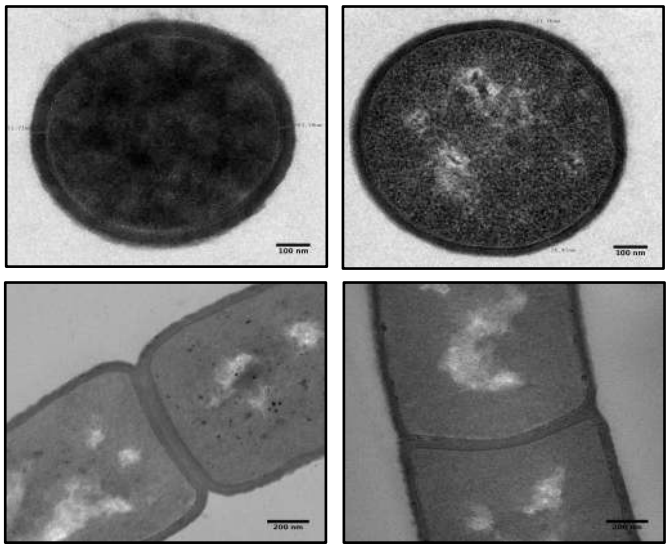

BAS WT

BAS Δ*prkC*

C

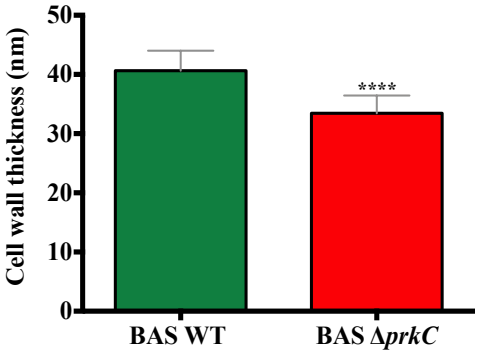

Figure 5 – figure supplement 1

A

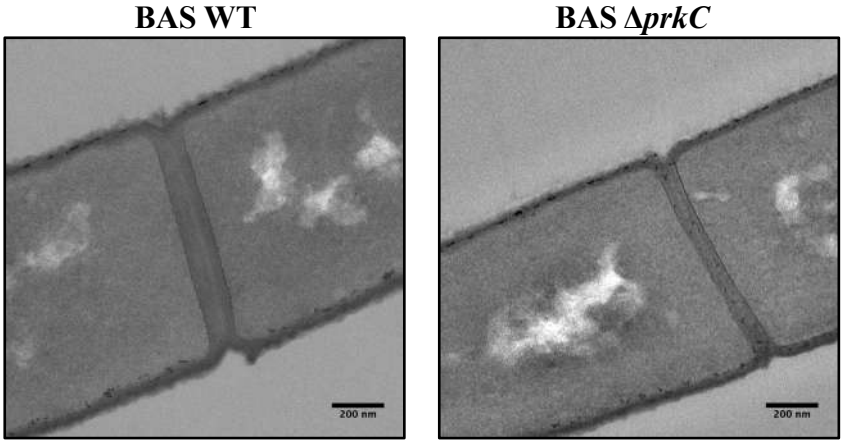

B

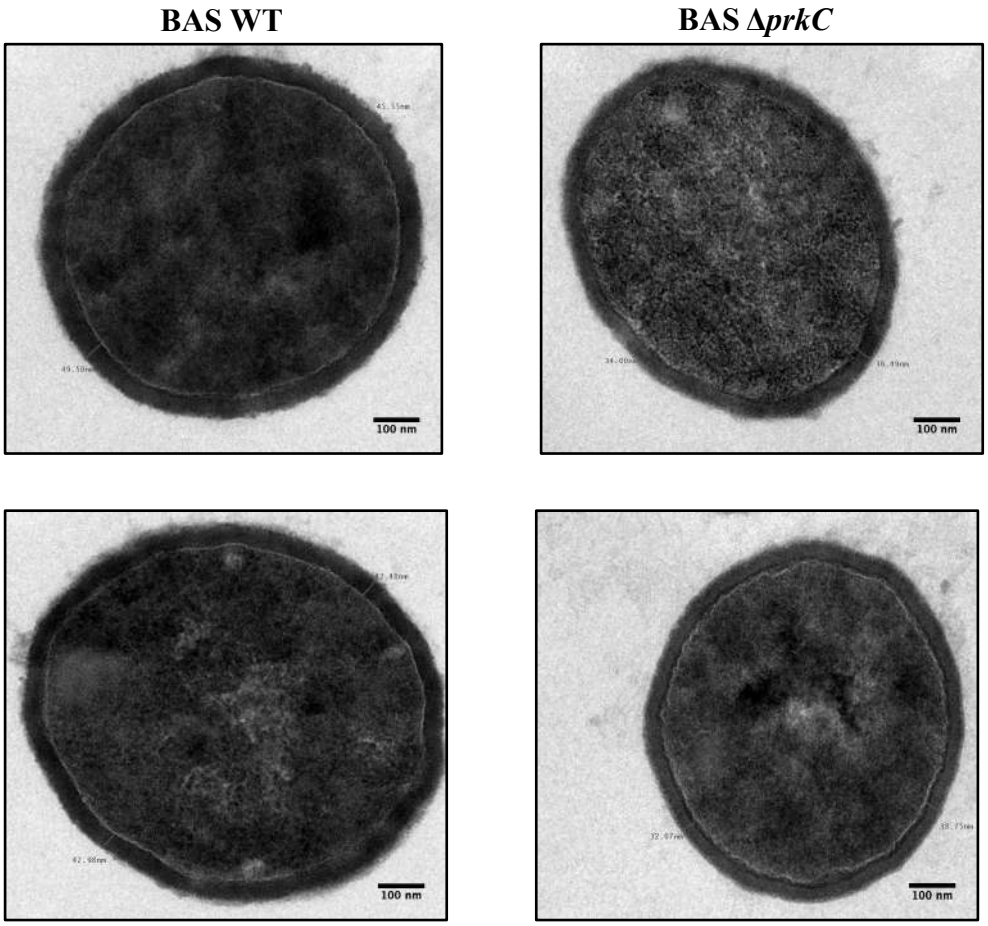

Figure 5 – figure supplement 2

Figure 5C: Summary statistics	
	Values
P Value	<0.0001
Summary	****
BAS WT Mean (nm)	40.63
BAS Δ*prkC* Mean (nm)	33.44
95% CI	8.101 to 6.276
R squared (eta squared)	0.5597

Figure 6

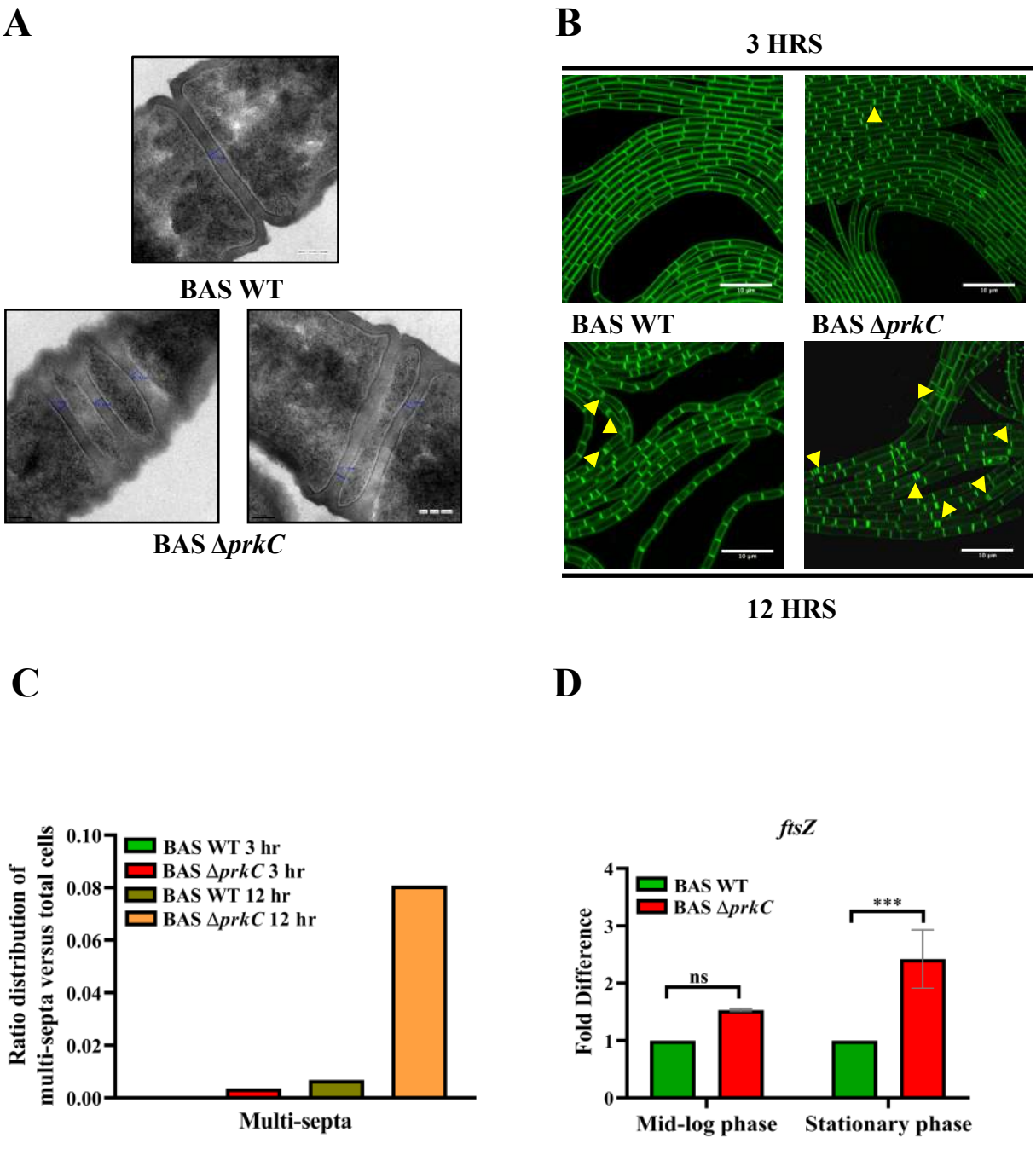
A
BAS WT
BAS ΔprkC
B
3 HRS
BAS WT
BAS ΔprkC
12 HRS
C
Ratio distribution of multi-septa versus total cells
0.10
0.08
0.06
0.04
0.02
0.00
BAS WT 3 hr
BAS ΔprkC 3 hr
BAS WT 12 hr
BAS ΔprkC 12 hr
Multi-septa
D
ftsZ
Fold Difference
4
3
2
1
0
BAS WT
BAS ΔprkC
ns
***
Mid-log phase
Stationary phase

Figure 6 – figure supplement 1

A

BAS WT

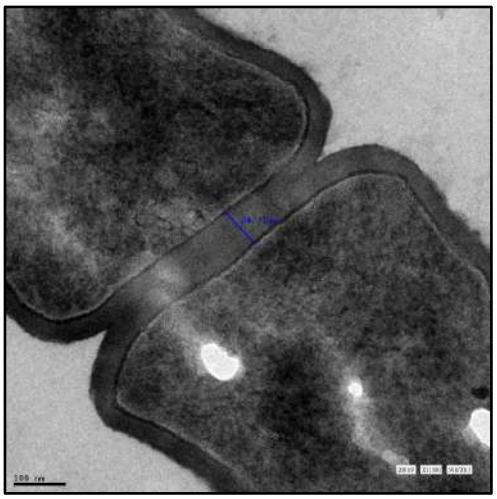

BAS Δ*prkC*

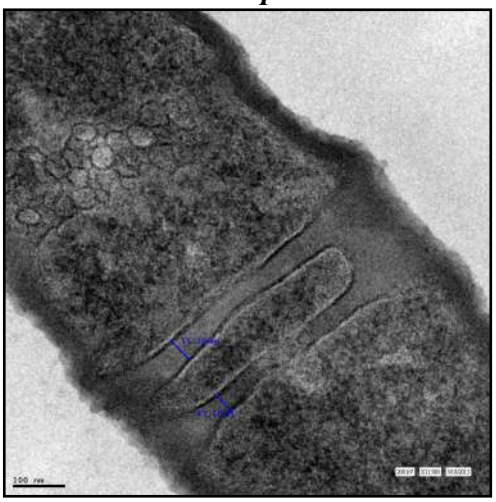

B

3 HRS

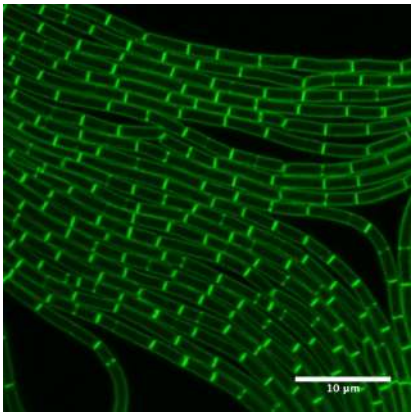

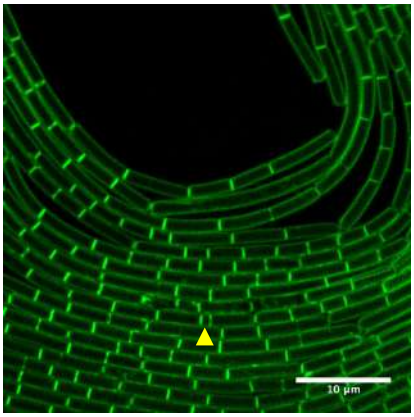

BAS WT

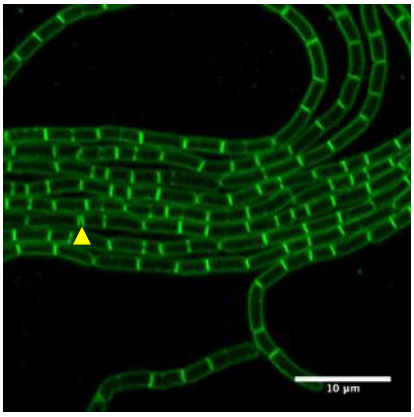

BAS Δ*prkC*

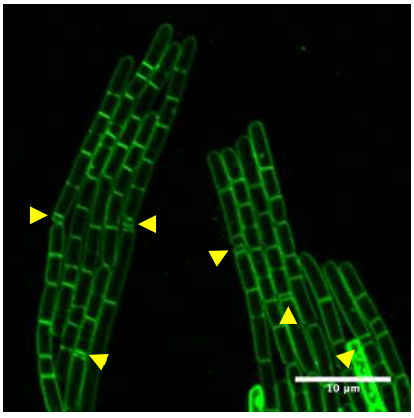

12 HRS

Figure 6 – figure supplement 2

Figure 6D : Summary statistics			
BAS WT- BAS Δ*prkC*	**95% CI of Difference**	**Summary**	**Adjusted P Values**
Mid-log phase	-1.102 to 0.03703	ns	0.0657
Stationary phase	-1.991 to -0.8526	***	0.0003

Figure S1

PrkC_B.anthracis
PrkC_B.cereus
PrkC_L.pneumophila
PrkC_S.pneumoniae
0.0
PrkC B.anthracis Sterne
1.4
0.0
PrkC B.cereus
0.0
1.3
PrkC S.pneumoniae
PrkC L.pneumophila
1.4
0.20

Supplementary Table S1

	Table S1. List of primers used in this study	
S. No	**Primer Name**	**Primer sequence 5´→ 3´**
Real time PCR primers		
P1	BAS 3757_ftsZ RT FP	TGCCTCTAACATTGGCGTGT
P2	BAS 3757_ftsZ RT RP	CAAGCGGCATCTGGTATTGC
P3	BAS0102 _rpoB_RT_FP	AACTTGCGCACATGGTTGAC
P4	BAS0102 _rpoB_RT_RP	CTGTCCACCGAACTGAGCTT
Primers for Protein Purification		
P5	BAS0841 Fp (BamHI)	GGGGGATCCCCATGGCAAAGACTAACTC
P6	BAS0841 Rp (XhoI)	GGGCTCGAGATTATTTTGTTGCAGGTTTTGC
P7	BAS0842 Fp (BamHI)	CCCGGATCCCCATGGCAAAGACTAACTCTTAC
P8	BAS0842 Rp (XhoI)	GGGCTCGAGTTATAGATTTGGGTTATTAAG
P9	BAS0253_groEL_BamHI_FP	AATCCAAGGGGGTGGATCCTTATGGCAAAAG
P10	BAS0253_groEL_XhoI_RP	TTAGGGCAAACTCGAGTTACATCATTCCGCCC
P11	BAS1683 FP (EcoRI)	CCCGAATTCATGAAAAAAGTTATTTCTAATGTG
P12	BAS1683 RP (XhoI)	CCCCTCGAGTTGTATTTTTAAGTTCTTCTTCAATGTCC
Primers for complement strain generation		
P13	Prkc Spe1 Fp	CCACTAGTCGTGCTGATTGGAAAACGCTTAAATG
P14	Prkc BamH1 Rp	CCGGATCCTTATTGTGTTGGATATGGTACTTCTTTG
P15	PrkC Promoter Kpn1 Fp	CCGGTACCATTGTCGGTCGTGGTACAGAAACTG
P16	PrkC promoter Spe1 Rp	CCACTAGTATGGCTCGTCCTCTTTCTTTTTC

Supplementary Table S2

Table S2. List of plasmids used in this study			
Name	**Description**	**Resistance Marker**	**Reference**
pYS5	Plasmid used for complementation in *B. anthracis*; AmpR in *E. coli*; KanR in *B. anthracis*	Kanamycin, Ampicillin	Singh et al., 1989
pYS5-prkC*	Plasmid expressing PrkC under own promoter in *B. anthracis*	Ampicillin, Spectinomycin	This study
pProExHTc	*E. coli* expression vector with N-terminal His_6-tag	Ampicillin	Invitrogen
pET28a	*E. coli* expression vector with N and C-terminal His_6-tag	Kanamycin	Invitrogen
pProExHTc-sap	Expression of His_6-Sap in *E. coli*	Ampicillin	This study
pProExHTc-eag	Expression of His_6-EA1 in *E. coli*	Ampicillin	This study
pProExHTc-groEL	Expression of His_6-GroEL in *E. coli*	Ampicillin	This study
pET28a-bslo	Expression of His_6-BslO in *E. coli*	Kanamycin	This study

Supplementary Table S3

Table S3. Bacterial strains used in this study			
Name	**Genotype**	**Resistance marker**	**Reference**
DH5α	*E. coli* F^{-} *endA1 glnV44 thi-1 recA1 relA1 gyrA96 deoR nupG purB2 0* φ80d*lacZ*ΔM15 Δ(*lacZYA-argF*)U169, hsdR17($r_K^{-}m_K^{+}$), λ^{-}	-	Invitrogen
BL21(DE3)	*E. coli* B strain: F^{-} *ompT gal dcm lon hsdS$_B$*($r_B^{-}m_B^{-}$) λ(DE3 [*lacI lacUV5-T7p07 ind1 sam7 nin5*]) [*malB*$^{+}$]$_{K-12}$(λ^{S})	-	Invitrogen
SCS110	*E. coli* SCS110 is an endA^{-} derivative of the JM110 strain *rpsL* (Strr) *thr leu endA thi-1 lacY galK galT ara tonA tsx dam dcm supE44* Δ(*lac-proAB*) [F′ *traD36 proAB lacI*qZΔ*M15*].	-	Stratagene
B. anthracis Sterne 34F2 (BAS WT)	*B. anthracis* strain pXO1^{+}, pXO2^{-}	-	NIAID, NIH
BAS Δ*prkC*	*B. anthracis* Sterne:: *prkC*	Kanamycin	Shah et al., 2008
BAS Δ*prkC::prkC*	*B. anthracis* Sterne:: *prkC* + *prkC*	Kanamycin, Spectinomycin	This study